Journal of Materials Chemistry B

PAPER

View Article Online
View Journal | View Issue

Cite this: J. Mater. Chem. B, 2019, 7, 415

Achieving traceless ablation of solid tumors without recurrence by mild photothermal-chemotherapy of triple stimuli-responsive polymer–drug conjugate nanoparticles†

Chang Du,[a] Yue Ding,[a] Jiwen Qian,[a] Rong Zhang[b] and Chang-Ming Dong *[ab]

Received 14th September 2018,
Accepted 5th December 2018

DOI: 10.1039/c8tb02432d

rsc.li/materials-b

Although photothermal therapy (PT) and photothermal-chemotherapy (PT-CT) treatments have been used to achieve complete ablation of solid tumors, they are often implemented at more than 50 °C under high intensity and using a high dose of NIR irradiation, concomitantly inducing heavy skin burning, tissue damage, and ugly scarring. Moreover, the residual tumor cells at the treated site cannot be completely eradicated, resulting in tumor recurrence and metathesis. These key obstacles have prohibited PT and PT-CT treatments from transitioning to clinical use, therefore achieving traceless ablation of solid tumors without recurrence is still a challenge for real applications. To balance hyperthermia and a high drug-loading capacity in polyprodrugs to achieve mild PT-CT, we rationally designed a novel type of intracellular pH and reduction-cleavable chlorambucil prodrug and synthesized high drug-loading polydopamine-chlorambucil conjugate nanoparticles (PDCBs). The PDCBs show good photothermal properties and demonstrate intracellular pH-, reduction-cleavable, and external near infrared (NIR)-triggered drug release profiles. Polydopamine-chlorambucil conjugate nanoparticles with 40 wt% CB ($PDCB_{40}$) and mild NIR irradiation could facilitate cellular internalization and subcellular trafficking, generating an excellent and synergistic antitumor effect *in vitro*. Pharmacokinetics and small animal fluorescent and photoacoustic imaging demonstrate that $PDCB_{40}$ has a 3.6-fold longer blood circulation time compared to free CB and attained selective tumor accumulation, simultaneously inducing a 4.1-fold stronger photoacoustic signal than the control. By using one intravenous injection of $PDCB_{40}$ and a single dose of mild NIR irradiation, this simple and mild PT-CT treatment achieved a non-discerned tumor on the sixth day, and traceless and complete ablation of a solid MCF-7 tumor without recurrence within 50 days, opening up a new avenue for precise cancer therapy with the potential for real applications.

1. Introduction

The near-infrared light (NIR, 650–950 nm) absorbing nanoparticles including inorganic carbon and gold nanostructures, transition-metal dichalcogenides, semiconducting polymers, melanin and polydopamine, to name just a few, can efficiently transduce laser irradiation to hyperthermia and achieve cancer photothermal therapy (PT) in a minimally invasive manner.[1–12] Compared with various cancer treatments including surgery, radiotherapy, chemotherapy (CT), and their cocktail therapies, this NIR-mediated PT treatment presents several advantages, such as: (1) achieving spatiotemporal manipulation, pinpoint tumor ablation, and a passive targeting effect to the tumor *via* the enhanced permeation and retention effect (EPR); (2) by thermally expanding the tumor blood vessels and enhancing the membrane permeability, the hyperthermia effect facilitates the extravasation, accumulation and penetration of nanoparticles in the tumor, and subsequent cellular internalization; and (3) this hyperthermia might induce antitumor immunity, improve the efficacy of CT, and generate a synergistic antitumor effect in the cocktail therapies.[13–16] Although most of the PT and PT-CT treatments have achieved complete ablation of solid tumors, they are often implemented at more than 50 °C under high intensity and a high dose of NIR irradiation, concomitantly inducing heavy and ugly scarring, skin burning, and damage to the surrounding normal tissue.[17–20] Moreover, the residual tumor cells in the

[a] School of Chemistry and Chemical Engineering, Shanghai Key Laboratory of Electrical Insulation and Thermal Aging, Shanghai Jiao Tong University, Shanghai 200240, P. R. China. E-mail: cmdong@sjtu.edu.cn
[b] Joint Research Center for Precision Medicine, Shanghai Jiao Tong University Affiliated Sixth People's Hospital South Campus, Shanghai Fengxian Central Hospital, Shanghai 201400, P. R. China

† Electronic supplementary information (ESI) available: Scheme S1, Table S1, S2 and Fig. S1–S15. See DOI: 10.1039/c8tb02432d

treated site cannot be completely eradicated, resulting in tumor recurrence and metathesis. These key obstacles prohibit PT and its cocktail treatments from transitioning to the clinic, and achieving traceless ablation of solid tumors without recurrence using mild PT (*i.e.*, mild photothermia under mild intensity and a dose of NIR irradiation) is urgently needed to enable real application of this widely studied PT technology.

In the case of very mild PT (*i.e.*, weak PT under a lower irradiation intensity and lower dose), a few examples from the published research have made progress in overcoming the above-mentioned obstacles. Liu *et al.* reported gambogic acid and indocyanine co-loaded coordination polymer nanofibers induced efficient tumor cell apoptosis at approximately 43 °C after 20 min of 808 nm irradiation at 0.3 W cm^{-2}, during which two out of five tumors were completely eradicated in a 14 day period with the assistance of gambogic acid to inhibit heat-shock protein production.[19] With 21 days of consecutive NIR irradiation (10 min, 850 nm, 0.4 W cm^{-2}), a very mild temperature of ~44 °C was used to achieve elimination of a 4T1 tumor using a pH-sensitive hemolytic polymer coated polydopamine (PDA), the tumor disappeared on the 15th day, within the 21 day therapeutic period.[20] Therefore, developing mild PT to achieve traceless and complete eradication of solid tumors without recurrence is still challenging, especially to provide simple method for use in the clinic (*i.e.*, simple treatment protocol including one intravenous injection with a single NIR irradiation dose).

In contrast to non-biodegradability and potentially long-term toxicity of inorganic nanomaterials, organic indocyanine green, porphysomes, natural melanin, and biomimetic PDA have attracted significant attention in the field of cancer PT owing to their good biodegradability and biocompatibility.[21–34] Owing to their simple self-polymerization (*i.e.*, one-pot synthesis of nanoparticles in a mild alkaline solution), good biocompatibility and biodegradability, and their biomimicry of melanin (*i.e.*, the hierarchical structure and NIR-absorbing function), the PDA and derived materials hold great promise in cancer PT, PT-CT, and theranostics. On the other hand, polymer–drug conjugates provide distinct attributes including variable drug-loading capacity, no leaking of the drug to be released, minimized side effects and an enhanced CT efficacy compared to the physically drug-loaded materials.[35–42] Several polymer–drug conjugates (or polyprodrugs) are being translated into the clinic, however, polyprodrugs with an intrinsic NIR-absorbing capacity and photo-mediated imaging functions (*e.g.*, photoacoustic imaging) are rarely constructed for use in precision cancer PT and PT-CT treatment.[43] To address the two key dilemmas in cancer PT and PT-CT treatments, that is, the first is that the high intensity and high dose of NIR irradiation induce heavy scarring, skin burning, and tissue damage, and the second is that the residual tumor cells in the treated site can result in tumor recurrence and metathesis, we put forward an innovative strategy of leveraging the hyperthermia and the high drug-loading capacity of polyprodrugs to achieve mild PT-CT. We rationally designed a novel dual stimuli-sensitive polydopamine-chlorambucil conjugate nanoparticles (PDCBs) that have a high drug-loading capacity and good NIR-absorbing attributes (Fig. 1), maximizing the intracellular physiological stimuli-triggered CT efficacy under mild photothermia (*i.e.*, endolysosome pH 5.0 and 10 mM DTT reduction to mimic the cytosolic glutathione gradient).[16,27,43–46] Using one intravenous injection and a single dose of mild NIR irradiation (808 nm, 1 W cm^{-2}, 10 min), the polyprodrug polydopamine-chlorambucil conjugate nanoparticles with a 40 wt% CB ($PDCB_{40}$) formulation generated a superior and synergistic antitumor efficacy and achieved complete and traceless ablation of a solid MCF-7 tumor that did not recur within 50 days, providing a simple, practical and mild PT-CT treatment for use in precision cancer therapy.

2. Experimental section

2.1 Materials

Acetone (99.5%), dichloromethane (99.5%), diethyl ether (99.5%), and methanol (99.5%) were distilled before use, respectively. Chloroambucil (CB, 98%, J&K), dicyclohexylcarbodiimide (DCC, 99.2%, Aldrich), 4-dimethylaminopyridine (DMAP, 99%, Adamas), 3,4-dihydroxy-benzenepropanoic acid (98%, Aldrich), 2,2′-dithiodiethanol (Alfa, 90%), D,L-dithiothreitol (DTT, 99%, J&K), dopamine hydrochloride (98%, Aldrich), phosphorus trichloride (99%, Aldrich), and trometamol (tris, ≥99.9%, Aldrich) were used as received. Trifluoroacetic acid (≥99%) was purchased from Shanghai Sinopharm Corp. Dulbecco's modified eagle medium (DMEM, PAA laboratories), fetal bovine serum (FBS, PAA laboratories), methylthiazolyldiphenyl-tetrazolium bromide (MTT, ultrapure, Aldrich), LysoTracker (ultrapure, Yeasen), and propidium iodide (PI, ultrapure, Yeasen) were used as received. L929 (a mouse fibroblastic cell line), HeLa (a human uterine cervix carcinoma cell line), and MCF-7 (a human breast carcinoma cell line) were received from Shanghai Institute of Biochemistry and Cell Biology.

2.2 Methods

Fourier transform infrared (FT-IR) spectroscopy was recorded on a Perkin Elmer Spectrum 100 spectrometer at room temperature. ^{1}H nuclear magnetic resonance (NMR) (400 MHz) and ^{13}C NMR (100 MHz) spectra were recorded on a Varian Mercury-400 spectrometer at room temperature using tetramethylsilane as an internal standard. Time-of-flight mass spectrometry (TOF-MS) was performed on a Waters Acquity UPLC/Premier QTOF MS Premier. X-ray photoelectron spectroscopy (XPS) was conducted on a VG ESCALAB MKII spectrometer and obtained by using XPS PEAK software (Version 4.1) to deconvolute the spectra. The mean hydrodynamic diameter and polydispersity index (PDI) of the nanoparticles were determined using dynamic light scattering (DLS), during which the samples were measured five times on a Malvern ZS90 instrument at 25 °C. Transmission electron microscopy (TEM) was performed on a JEM-2010 instrument at a 200 kV accelerating voltage, during which the samples were dropped onto 300 mesh Formvar-carbon film-coated copper grids. The UV-Vis-NIR spectroscopy was recorded on a

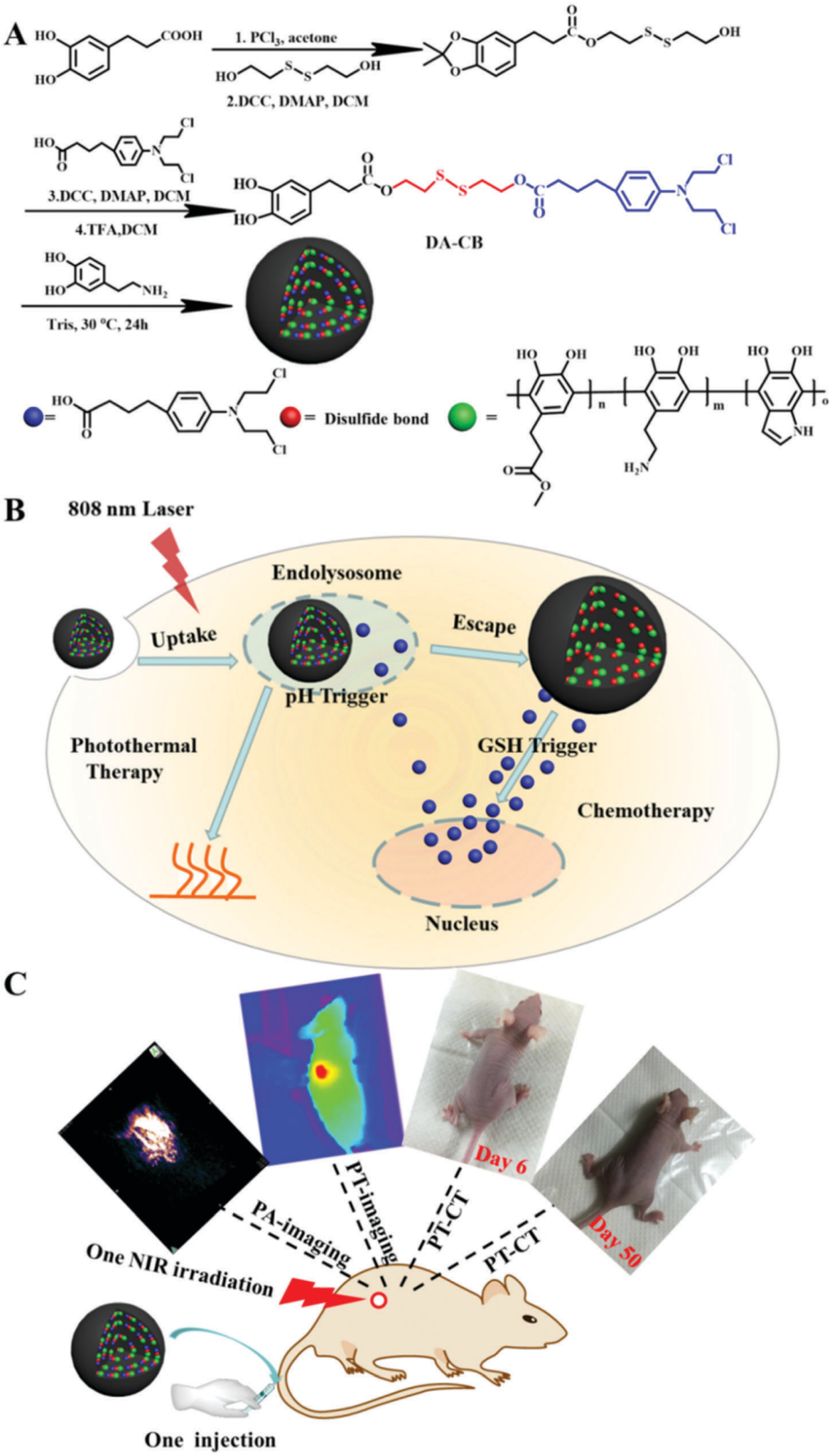

Fig. 1 Synthesis of the prodrug dopamine-chloroambucil (DA-CB) and the PDCBs conjugate nanoparticles (A). The cellular uptake of the PDCBs, intracellular pH and GSH cleavable CB release, and the synergistic PT-CT upon mild NIR irradiation (B). Illustration showing mild PT-CT treatment with one injection and one dose of NIR irradiation and both PT and PA imaging *in vivo* (C).

Perkin-Elmer Lambda 750S spectrometer at room temperature. The fluorescent spectroscopy was recorded on a Perkin-Elmer LS-50B spectrometer at room temperature. All of the 808 nm NIR irradiation was carried out by using a continuous wave diode laser (Shanghai SFOLT Corp., FC-960-6000-MM) with tunable power (0–1650 mW), during which the spot size was tuned using a fiber collimator connected by a fiber optic patch cable (FC/PC/200UM/1M).

2.3 Synthesis of the chloroambucil prodrug of dopamine-chloroambucil

The dual stimuli-sensitive prodrug dopamine-chloroambucil (DA-CB) was synthesized using the following four steps. Firstly, 3,4-dihydroxybenzenepropanoic acid (DBA, 1.0 g, 5.49 mmol) was dissolved in dry acetone (20 mL) at 0 °C. Phosphorus trichloride (383 μL, 4.4 mmol) was then slowly added dropwise into the above solution and the reaction mixture was vigorously stirred for 6 h at 0 °C. The acetone was removed by rotary evaporation and the residues were dissolved in diethyl ether (10 mL). The organic layer was extracted using water three times and then concentrated to give 2,2-dimethyl-1,3-benzodioxole-5-propanoic acid (65% yield).[47] ^{1}H NMR (400 MHz, $CDCl_3$), δ (ppm) = 1.60 (s, 6H, (CH_3)$_2$), 2.47 (dd, J = 7.6, 4.8 Hz, 2H, CCH_2CH_2COOH), 2.71 (dd, J = 7.6, 7.6 Hz, 2H, CCH_2CH_2-COOH), 6.70–6.60 (m, 3H, **Ar**). ^{13}C NMR (100 MHz, DMSO-d_6), δ (ppm) = 174.28 (C═O), 147.26 (Ar), 145.53 (Ar), 134.50 (Ar), 120.91 (Ar), 117.96 **C**(CH_3), 108.95 (Ar), 108.23 (Ar), 36.05 (Ar-CH_2), 30.59 (CH_2CO), 25.99 C(CH_3). FT-IR (KBr, cm^{-1}): 2981 (ν_{C-H}), 1707 (ν_{COOH}), 1609, 1498 (ν_{phenyl}), 1122 (ν_{C-O-C}).

Secondly, 2,2-dimethyl-1,3-benzodioxole-5-propanoic acid (1 mmol, 222.0 mg), DMAP (1 mmol, 122.2 mg), and DCC (1 mmol, 206.0 mg) were dissolved in dichloromethane (5 mL) and stirred for 4 h at room temperature under nitrogen atmosphere. Then the above solution was added dropwise into 2,2′-dithiodiethanol (3 mmol, 396.5 mg) in dichloromethane (1 mL) and the reaction mixture was vigorously stirred for another 48 h under a nitrogen atmosphere at room temperature. Dichloromethane was removed by rotary evaporation and the residues were purified using silica column chromatography (dichloromethane: methanol, 50 : 1) to give the intermediate product (70% yield). ^{1}H NMR (400 MHz, CD3OD-d_4), δ (ppm) = 1.60 (s, 6H, (CH_3)$_2$), 2.60 (dd, J = 7.2, 7.6 Hz, 2H, $ArCH_2CH_2$), 2.83 (m, 4H, CH_2S–SCH_2), 2.90 (dd, J = 6.4, 6.4 Hz, 2H, $ArCH_2$), 3.77 (dd, J = 6.4, 6.4 Hz, 2H, S–SCH_2CH_2OH), 4.31 (dd, J = 6.4, 6.4 Hz, 2H, S–SCH_2CH_2O), 6.60 (m, 3H, **Ar**). ^{13}C NMR (100 MHz, $CDCl_3$), δ (ppm) = 173.02 (C═O), 148.37 (Ar), 148.16 (Ar), 133.93 (Ar), 120.51 (Ar), 117.22 [**C**(CH_3)], 108.65 (Ar), 107.70 (Ar), 62.00 (CO–C–CH_2), 60.00 (CH_2OH), 40.88 (SCH_2CH_2OH), 37.07 (SCH_2CH_2O), 35.97 ($ArCH_2CH_2$), 30.18 ($ArCH_2CH_2$), 24.56 [C(CH_3)]. FT-IR (KBr, cm^{-1}): 2981 (ν_{C-H}), 1736 (ν_{COO}), 1608, 1498 (ν_{phenyl}), 1076 (ν_{C-O-C}).

Thirdly, chloroambucil (CB, 0.5 mmol, 152.0 mg), DMAP (0.5 mmol, 61.1 mg), and DCC (0.5 mmol, 103.0 mg) was dissolved in dichloromethane (5 mL) and stirred for 4 h at room temperature under a nitrogen atmosphere, and then the above solution was added dropwise into the above-obtained intermediate (0.5 mmol, 179.0 mg) in dichloromethane (1 mL). The reaction mixture was vigorously stirred for another 48 h under a nitrogen atmosphere at room temperature. Dichloromethane was removed by rotary evaporation and the residues were purified using silica column chromatography (dichloromethane) to give the product (85% yield). ^{1}H NMR (400 MHz, CD_3OD), δ (ppm) = 1.60 (s, 6H, (CH_3)$_2$), 1.90 (m, 2H, $CCH_2CH_2CH_2$-Ar), 2.38 (dd, J = 7.6, 7.2 Hz, 2H, $CCH_2CH_2CH_2$-Ar), 2.57 (m, 4H, $CCH_2CH_2CH_2$-Ar and CCH_2CH_2-Ar), 2.87 (m, 6H, CH_2SSCH_2 and CCH_2CH_2-Ar), 3.60–3.68 (m, 4H, N(CH_2CH_2Cl)$_2$), 4.32 (m, 4H, $CH_2CH_2SSCH_2CH_2$), 6.60 (m, 5H, **Ar**), 7.07 (m, 2H, **Ar**). ^{13}C NMR (100 MHz, CD_3OD), δ (ppm) = 173.55 (**C**OO), 172.81 (OO**C**), 147.70 (Ar), 145.88 (Ar), 144.48 (Ar), 133.27 (Ar), 130.94 (Ar), 129.80 (Ar), 120.52 [**C**(CH_3)], 117.69 (Ar), 112.57 (Ar), 111.83 (Ar), 109.11 (Ar), 107.72 (Ar), 62.30 ($COOCH_2$) 61.02 (CH_2COO), 53.81 (CH_2Cl), 53.51 (CH_2Cl), 40.91 (NCH_2), 40.45 (NCH_2), 37.43 (SCH_2), 37.42 (CH_2S), 36.49 ($ArCH_2$-CH_2CO), 34.38 ($ArCH_2CH_2CH_2CO$), 33.21 ($ArCH_2CH_2CH_2CO$), 29.98 ($ArCH_2CH_2CO$), 26.92 ($CH_2CH_2CH_2$), 25.82 [C(CH_3)]. FT-IR (KBr, cm^{-1}): 2981 (ν_{C-H}), 1732 (ν_{COO}), 1613, 1518 (ν_{phenyl}), 1076 (ν_{C-O-C}), 802 (ν_{C-Cl}).

Finally, the above-obtained product (0.5 mmol, 322.0 mg) was dissolved in dichloromethane (5 mL) and then TFA (5 mL) was added dropwise and stirred for 24 h at room temperature. The target product of DA-CB was quantitatively obtained. ^{1}H NMR (400 MHz, CD_3OD), δ (ppm) = 1.90 (m, 2H, $CCH_2CH_2CH_2$-Ar), 2.33 (dd, J = 7.6, 7.2 Hz, 2H, $CCH_2CH_2CH_2$-Ar), 2.57 (m, 4H, $CCH_2CH_2CH_2$-Ar and CCH_2CH_2-Ar), 2.87 (m, 6H, CH_2SSCH_2 and CCH_2CH_2-Ar), 3.60–3.68 (m, 4H, N(CH_2CH_2Cl)$_2$), 4.32 (m, 4H, $CH_2CH_2SSCH_2CH_2$), 6.60 (m, 5H, **Ar**), 7.07 (m, 2H, **Ar**). ^{13}C NMR (100 MHz, $CDCl_3$), δ (ppm) = 174.88 (C1), 174.49 (C2), 144.00 (C3), 142.47 (C4), 139.97 (C5), 136.74 (C6), 133.18 (C7), 130.53 (C8, C9), 120.94 (C10), 116.12 (C11, C12), 115.39 (C13,C14), 62.63 (C15, C16), 56.11 (C17, C18), 39.06 (C19, C20), 37.39 (C21), 36.23 (C22), 34.36 (C23), 33.70 (C24), 30.44 (C25), 29.13 (C26), 26.56 (C27). FT-IR (KBr, cm^{-1}): 3409 (broad, ν_{OH}), 2981 (ν_{C-H}), 1732 (ν_{COO}), 1615, 1519 (ν_{phenyl}), 806 (ν_{C-Cl}). TOF-MS: calculated, 604.1361 [M + H]; found, 604.1376 [M + H]$^+$.

2.4 Synthesis of the PDCBs conjugate nanoparticles

The PDCBs conjugate nanoparticles (the subscript denotes the weight percentage of the CB) and the control PDA ones were synthesized according to the method described in our previous publication, respectively.[43] As a typical example, both DA-CB (53.7 mg) and DA hydrochloride (12.5 mg) were pre-dissolved in deionized water (1 mL) and were then added into an aqueous solution (20 mL) of tris (410.0 mg) at 30 °C, and then stirred under air for 24 h. The resultant suspension was dialyzed (molecular weight cutoff: 3500) against deionized water or PBS (10 mM, pH 7.4) for 2 days to give the nanoparticles in solution and then stored at −4 °C for further use.

In addition, to prepare the DOX-loaded $PDCB_{40}$ for small animal fluorescent imaging, 2 mg $PDCB_{40}$ was dispersed in PBS, followed by the addition of 3 mL of DOX in PBS (1 mg mL^{-1}) and this was stirred at room temperature for 24 h. Then DOX-loaded $PDCB_{40}$ was harvested by immediate centrifugation (10 min, 15 000 rpm) and then washed using PBS three times. The DOX

content was determined at 480 nm absorbance using UV-Vis spectroscopy and repeated six times.

2.5 NIR-mediated photothermal property of PDCBs

Generally, 200 μL of the PDCBs solution with different concentrations was added in a 96-well plate and then irradiated using the NIR laser (808 nm, 1, 2, 4 W cm^{-2}, 10 min), during which the solution temperature and the repeated heating–cooling cycles (*i.e.*, 10 min NIR irradiation and 10 min naturally cooling) were recorded using a digital thermometer every 30 s, respectively.

2.6 *In vitro* chloroambucil release

For the DTT, pH, and the DTT + pH triggered release, the PDCBs in PBS (1 mL, 10 mM, pH 7.4) with/without 10 mM DTT were transferred into a dialysis bag (MWCO = 3500 Da), and then incubated in 10 mL of PBS at different pH values (*i.e.*, pH 5.0 and 7.4) at 37 °C. For the NIR-triggered release, the samples were vertically irradiated using the NIR laser (808 nm, 1 W cm^{-2}, 10 min) at 0.5, 1, 2, 4, 6, 8, 10, 12 h and then put into 10 mL of PBS with a constant shaking rate of 150 rpm at 37 °C. Then, 10 mL of dialysis solution was taken out at predetermined time intervals and the same volume of fresh PBS was added back. The released CB was measured by the absorbance at 258 nm using a UV-Vis spectrophotometer. All release experiments were carried out in duplicate and each sample was measured three times. In addition, the molecular structure of the released drug from the nanoparticles was confirmed using TOF-MS.

2.7 *In vitro* PT, CT, and PT-CT

The L929, HeLa, and MCF-7 cell lines were cultured at 37 °C in DMEM supplemented with 10% FBS, 100 IU per mL penicillin, and 100 μg per mL streptomycin under a humidified atmosphere of 5% CO_2. L929 was only used to evaluate the cytotoxicity of the PDA and the latter two carcinomas were used to measure the cytotoxicity and antitumor activity. Briefly, the cells were seeded into 96-well plates (10^4 cells per well) in 200 μL of culture medium and incubated overnight at 37 °C. 200 μL of PDA or PDCBs with gradient concentrations were added and then incubated for 48 h. After twice washing with fresh culture medium and PBS, 20 μL of the 5 mg mL^{-1} MTT stock solution in PBS was added to each well and further incubated for 4 h to allow full formation of formazan. Finally, the blue formazan was dissolved in 100 μL DMSO for 20 min and the absorbance at 490 nm was measured using a Microplate Reader (Elx800, BioTek Company).

To evaluate the PT and PT-CT, nanoparticle solutions with gradient concentrations were added separately into a 96-well plate and incubated for 4 h at 37 °C prior to the NIR irradiation (808 nm, 1 W cm^{-2}, 10 min). The cells were further incubated for 12 h for PT and 48 h for PT-CT, respectively, and then the MTT assay was used to determine the cell viability. The half maximal inhibitory concentration (IC_{50}) was calculated using GraphPad Prism 6 software from eight samples. As for the single CT and the combination CT, the IC_{50} was calculated on the basis of the CB concentration; and the IC_{50} values for the single PT and the combination PT were calculated on the basis of the concentration of pure PDA or PDA in the PDCBs. The combination index (CI) was calculated using the following equation: CI = [IC_{50} (combination CT)/IC_{50} (CT)] + [IC_{50} (combination PT)/IC_{50} (PT)].[48–51] All cell viabilities were tested using six replicates.

2.8 Cell internalization

Using MCF-7 as the model cell line, the cell internalization process of the free CB or $PDCB_{40}$ was studied using flow cytometry (CB: excitation at 345 nm and emission at 435 nm, BD Accuri C6) and inverted fluorescence microscopy (LeicaDMI6000 B). Briefly, MCF-7 was incubated in a 6-well plate (5.0×10^5 cells per well) for 24 h. The same drug concentration of free CB or $PDCB_{40}$ (10 μg mL^{-1} CB equivalent) was added to each well for a predetermined time at 37 °C with or without the NIR irradiation. The cells were rinsed with PBS, disposed with trypsin, and then the data collected for the 1.0×10^4 gated events were analyzed using FlowJo software. After similar treatment, MCF-7 was fixed with 4% formaldehyde for 30 min at room temperature, washed with PBS, stained using PI for 15 min, and then observed and analyzed using ImageJ software.

2.9 Intracellular trafficking of PDCBs

Intracellular trafficking and distribution of $PDCB_{40}$ was observed using confocal laser scanning microscopy (CLSM). Briefly, MCF-7 was incubated in 6-well plates (5.0×10^5 cells per well) for 24 h, replaced with fresh culture medium, then followed by addition of $PDCB_{40}$ at 10 μg mL^{-1} CB equivalent. After 2 h incubation, the medium was removed and the cells were irradiated using the NIR laser (808 nm, 1 W cm^{-2}, 10 min). The cells were rinsed with PBS three times and both cell nuclei and lysosomes were counterstained with PI (red) and LysoTracker (green), respectively. Finally, the cells were washed with PBS three times and observed using CLSM. The data were analyzed using ImageJ software. A control, without irradiation, was also carried out under same conditions.

2.10 Animals

Five week-old male Balb/c nude mice (~20 g) and Sprague-Dawley (SD) rats (~200 g) were purchased from the Chinese Academy of Sciences (Shanghai, China). The animal experiments were performed in accordance with the guidelines for the care and use of laboratory animals and approved by the Animal Ethics Committee of Shanghai Jiao Tong University.

2.11 Pharmacokinetics

The SD rats were randomly divided into two groups (n = 4) and each mouse was injected *via* the tail vein with 8 mg kg^{-1} free CB or a $PDCB_{40}$ equivalent. Blood samples (0.3 mL) were obtained *via* eye puncture at selected time intervals (*i.e.*, 0.25, 0.5, 1, 2, 4, 6, 8, 12, 14 and 24 h). Plasma samples were harvested by immediate centrifugation (10 min, 3000 rpm), frozen at −20 °C, and then the CB in the blood serum was analyzed using

fluorescence spectroscopy. The pharmacokinetic parameters were calculated using OriginPro 8.

2.12 *In vivo* multiple imaging and biodistribution

MCF-7 tumor-bearing nude mice with a tumor volume of approximately 300 mm^3 were intravenously injected *via* the tail vein with 200 μL of DOX-loaded $PDCB_{40}$ (1 mg mL^{-1}) or free DOX (5.3 mg kg^{-1}). *In vivo* fluorescent imaging was monitored at 1, 2, 4, 6, 8, 10, 12, 14 and 24 h post-injection using a Kodak multimode imaging system (DOX: excitation wavelength = 530 nm, emission wavelength = 600 nm). For the *ex vivo* distribution, after the mice were sacrificed by cervical vertebra dislocation at 2, 6 and 10 h post-injection (n = 3), all tumor and major organs were carefully collected, washed with saline, and then imaged using a Kodak multimode imaging system. Tissue samples were rinsed in saline, blotted using a paper towel, weighed and stored at −80 °C. After being homogenized in 0.5 mL of 1% Triton X-100, 1.2 mL of the extraction solution (HCl-IPA) was added and then incubated at −20 °C overnight. After vortexing and centrifugation at 15 000 × g for 15 min, the DOX amount measured using fluorescence spectroscopy is given as the percentage injected dose per gram of tissue (% ID/g).

For the *in vivo* hyperthermia and imaging, the mice (n = 4) were intravenously injected with 200 μL (2 mg mL^{-1}) of $PDCB_{40}$, PDA or the control PBS, and then irradiated using the NIR laser (808 nm, 1 W cm^{-2}, 10 min) at 10 h post-injection. The thermographic image and the temperature of the tumor site were recorded using an infrared thermal camera (AXT100, Ann Arbor Sensor Systems).

After $PDCB_{40}$ (200 μL, 1 mg mL^{-1}) or the control PDA was intravenously injected into the mice (n = 3), photoacoustic (PA) imaging was acquired at 1, 2, 4, 6, 8, 10, 12, 14 and 24 h post-injection using a commercial Endra Nexus 128 PA tomography system (Endra Inc., Ann Arbor, Michigan) equipped with a tunable nanosecond pulsed laser (808 nm, 7 ns pulse, 7 mJ per pulse, 2 Hz pulse repetition frequency) and a 128 unfocused ultrasound transducer with a 5 MHz center frequency. The PBS alone was used to eliminate the background signal for obtaining the PA signal of the PDA and/or PDCBs.

2.13 *In vivo* antitumor activity

The MCF-7 tumor-bearing mice with a tumor volume of 60–80 mm^3 were randomly divided into seven groups (n = 4) for antitumor studies. All of the mice were intravenously injected once at a time point of 0 days with 8 mg kg^{-1} CB, nanoparticles (PDA or $PDCB_{40}$, 200 μL, 2 mg mL^{-1}) or PBS. For the PDA + NIR and $PDCB_{40}$ + NIR groups, the tumor sites were irradiated using the NIR laser (808 nm, 1 W cm^{-2}, 10 min) at 10 h. The tumor size and body weight of each mouse were measured by using a caliper or a balance every two days. Tumor volume (V) was calculated according to the following equation: V (mm^3) = 1/2 × length (mm) × width (mm) × width (mm). The tumor inhibitory rates (TIR) of various treatments were calculated using the equation: TIR (%) = 100 × (mean tumor volume of the PBS group − mean tumor volume of others)/(mean tumor volume of the PBS group). Data are represented as the average ± standard error. When the tumor volume of the PBS group reached approximately 1500 mm^3 on day 32, one mouse from each group was sacrificed for comparative studies. Finally, the tumors, as well as the major organs (heart, liver, spleens, lung and kidneys), were dissected, washed with saline, weighed, photographed, and fixed with 4% formaldehyde for histology, TUNEL, and PCNA assays. All of the mice were euthanized if the tumor volume was larger than 1500 mm^3 or if the body weight loss was greater than 15%. Statistical analyses were performed using GraphPad Prism software 5.0 and data were given as mean ± S.D.

2.14 Statistical analysis

The two-way analysis of variance and the t-test were used to determine the statistical significance. A probability (P) value < 0.01 was considered significant, and P < 0.001 was highly significant. All computations were made by employing Microsoft Excel 2007.

3. Results and discussion

3.1 Synthesis of dual stimuli-sensitive polydopamine-chloroambucil conjugate nanoparticles (PDCBs)

As the disulfide bond is stable in physiological media and can be cleaved by the GSH gradient inside the cell environment, we selected it to connect 3,4-dihydroxybenzenepropanoic acid with an anticancer drug CB to afford a dopamine-derived prodrug DA-CB.[44–46] Meanwhile, 2,2′-dithiodiethanol containing a disulfide bond bridge was directly linked to the carboxy group of CB *via* an ester bond, which endowed the prodrug DA-CB with a subcellular (*e.g.*, endolysosome, pH = 4.5–6.5) acid-labile linker of β-thioethyl methanoate.[38,45] Thus, the prodrug DA-CB was expected to be cleaved by physiologically related dual stimuli triggers (*i.e.*, intracellular pH and GSH), which was rationally designed and synthesized using four steps and its molecular structure was fully characterized by means of FT-IR, ^{1}H NMR, ^{13}C NMR, and TOF-MS spectroscopy (Fig. 2A and B and Fig. S1, ESI†). The ^{1}H NMR spectroscopy for DA-CB shows proton signals at 4.32 ppm (m, 4H, –COO–C**H**$_2$CH$_2$–S–S–CH$_2$C**H**$_2$–OOC–) which can be assigned to the methylene linked to the carboxylic ester and the disulfide bond and those at 3.60–3.68 ppm (m, 4H, –N(C**H**$_2$C**H**$_2$Cl)$_2$) can be assigned to CB. The ^{13}C NMR spectroscopy presents the carbon signal of methylene at 62.63 ppm (–COO–***C***H$_2$CH$_2$–S–S–CH$_2$***C***H$_2$–OOC–), those at 174.88 ppm and 174.49 ppm represent the two carboxylic esters, and those at 56.11 ppm [–N(CH$_2$***C***H$_2$Cl)$_2$] and 39.06 ppm [–N(***C***H$_2$CH$_2$Cl)$_2$] represent the CB. Moreover, the TOF-MS confirms the prodrug DA-CB has an observed value of 604.1376 for $[M + H]^+$, which matches well with the theoretical value of 604.1361.

The oxidative self-polymerization and copolymerization of the dopamine and its derivatives allow the direct formation of the negatively charged PDA and the related nanoparticles in weakly basic water (*e.g.*, tris and $NH_3{\cdot}H_2O$).[21–24,43] Thereafter, the PDCBs were prepared using the precipitation copolymerization of

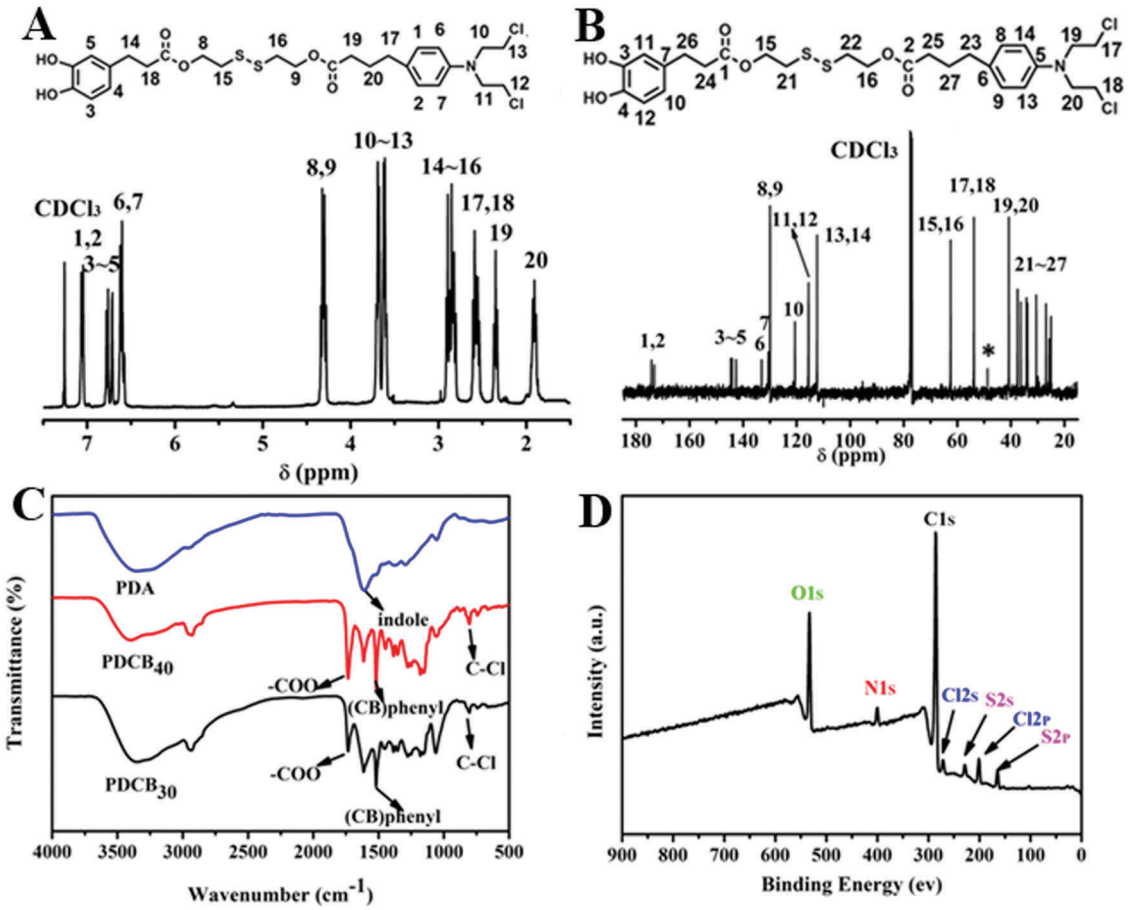

Fig. 2 ^{1}H NMR (A) and ^{13}C NMR (B) spectra for the DA-CB prodrug, FT-IR (C) of PDCBs and PDA, and XPS (D) for $PDCB_{40}$.

Table 1 Characterization of the PDCBs and PDA nanoparticles

Sample[a]	Diameter[b] (nm)	TEM morphology	Zeta potential[b] (mV)	IC_{50} (PT)[c] (μg mL^{-1})	IC_{50} (CT)[c] (μg mL^{-1})	IC_{50} (PT-CT)[d] (μg mL^{-1})	CI[e]
PDA	75 ± 3	Sphere	−33.1	53.76 (HeLa)	—	—	—
				69.34 (MCF-7)			
$PDCB_{30}$	126 ± 5	Sphere	−32.1	53.76 (HeLa)	14.15	8.42 + 3.61	0.41
				69.34 (MCF-7)	9.92	8.45 + 3.62	0.49
$PDCB_{40}$	154 ± 1	Sphere	−30.2	53.76 (HeLa)	14.03	5.54 + 3.69	0.37
				69.34 (MCF-7)	9.72	5.23 + 3.49	0.43

[a] The subscript denotes the weight percentage of CB within the PDCBs. [b] The mean diameter and the zeta potential of the nanoparticles in PBS are determined using DLS. [c] IC_{50} is calculated from Fig. 6 and Fig. S10 (ESI) by using GraphPad Prism 6 software; note that the IC_{50} (PT) for a single PT of PDCBs has to be substituted by PDA as an equivalent otherwise it would be disturbed by the PDCBs release induced CT. [d] For the combination PT-CT, the former value denotes the combination PT and the latter one is the combination CT. [e] CI denotes the combination index of PT-CT, and CI = [IC_{50} (combination CT)/IC_{50} (CT)] + [IC_{50} (combination PT)/IC_{50} (PT)].[48–51]

DA-CB with DA in Tris aqueous solution at 30 °C for 24 h and the detailed results are summarized in Table 1 and Table S1 (ESI†). The PDCBs have a higher NIR-mediated temperature-elevating ability (ΔT), which would induce a heterogenous and quick photothermal heating effect, resulting in heavy skin and tissue damage during the PT process.[17–20] Moreover, the PDA content within the PDCBs will play a decisive role in achieving a higher ΔT.[43] Therefore, we want to rationally endow the PDCBs with a mild ΔT and a higher drug-loading capacity. Taking the ΔT and the drug-loading capacity into consideration, both the $PDCB_{30}$ and $PDCB_{40}$ were used for the following studies (Table 1 and Table S2, ESI†).

The as-synthesized PDCBs were fully characterized by means of FT-IR, XPS, DLS, and TEM. Compared to the pure PDA counterpart, the FT-IR spectra for the PDCBs show a characteristic vibration peak at 1732 cm^{-1} for the ester carbonyl (–COO–) and one fingerprint signal at 804 cm^{-1} for CB (C–Cl), along with the indole peaks of PDA at 1625–1640 cm^{-1} (Fig. 2C). XPS analysis confirmed that the PDCBs had a comparative CB weight percentage to that in the feed ratio (Fig. 2D). This indicates that the prodrug DA-CB could be rationally copolymerized with DA to produce the polyprodrug type PDCBs. Specifically, the XPS of the PDCBs shows the binding energy peaks of –S–S– at 163.7 eV,

–COO– at 533.5 eV, and C–Cl at 201.7 eV, verifying the disulfide bond, the carboxylic ester linker and the CB drug are retained in the PDCBs (Fig. S2 and S3, ESI†). As shown in Fig. 3 and Fig. S4 (ESI†), both the DLS and TEM analyses show that the PDCBs have an almost spherical morphology with hydrodynamic diameters ranging from 120 to 150 nm, and the size determined using TEM is basically consistent with that measured using DLS. The size and morphology of the control PDA was characterized using similar methods and is shown in Fig. S5 (ESI†). Taken together, the PDA-based polyprodrug PDCBs with physiologically related dual stimuli triggers and a higher drug-loading capacity can be successfully prepared in a one-pot synthesis from the oxidative precipitation copolymerization of the prodrug DA-CB with DA.

After the nanoparticles enter into the bloodstream *in vivo*, the blood proteins nonspecifically absorb onto the surfaces of the nanoparticles to form a so-called protein corona, inducing aggregation, phagocytosis owing to the mononuclear phagocyte system, and even final clearance.[35–37] The PDCBs were dispersed well in PBS (10 mM, pH 7.4) at 4 °C or incubated with FBS (1%, 5%, and 10%) at 37 °C and their physiological stability was monitored using DLS (Fig. 3B). The PDCBs in FBS remained stable showing no obvious changes in 8 h and then increased to <250 nm after 24 h incubation, on the other hand, the PDCBs in PBS hardly changed for two months at 4 °C (Fig. S4C, ESI†). The PDCBs have a negative zeta potential of about 30.2–32.1 mV, enabling them to remain relatively stable in FBS at 37 °C despite the inevitable albumin absorption.

3.2 Photothermal effect and multi-stimuli-triggered drug release of PDCBs

Generally speaking, native melanin and the PDA-based nanomaterials have a NIR absorption of 650–900 nm because of their hierarchical structures, including the π–π stacking of the indole units, charge transfer, and the π-electron radicals localized to the quinone residues.[21–25] The UV-Vis-NIR spectra of the PDCBs present a broad and strong NIR-absorption at 650–900 nm in addition to a characteristic UV signal for the CB at 225 nm (Fig. 4A), and the NIR absorbance showed no observable difference before and after mild NIR irradiation (808 nm, 1 W cm^{-2}, 10 min). These data demonstrate that the PDCBs possess an intrinsic photothermal conversion capability and a good photothermal stability. Upon mild NIR irradiation, both the $PDCB_{30}$ and $PDCB_{40}$ solutions were heated by 13.9 °C and 12.8 °C, respectively, in comparison to the control PBS which was only heated by 2.5 °C (Fig. 4B). Moreover, the heating–cooling cycle curves were repeated three times with a negligible ΔT change (Fig. 4C). This data suggests that the PDCBs have good photostability, which is also

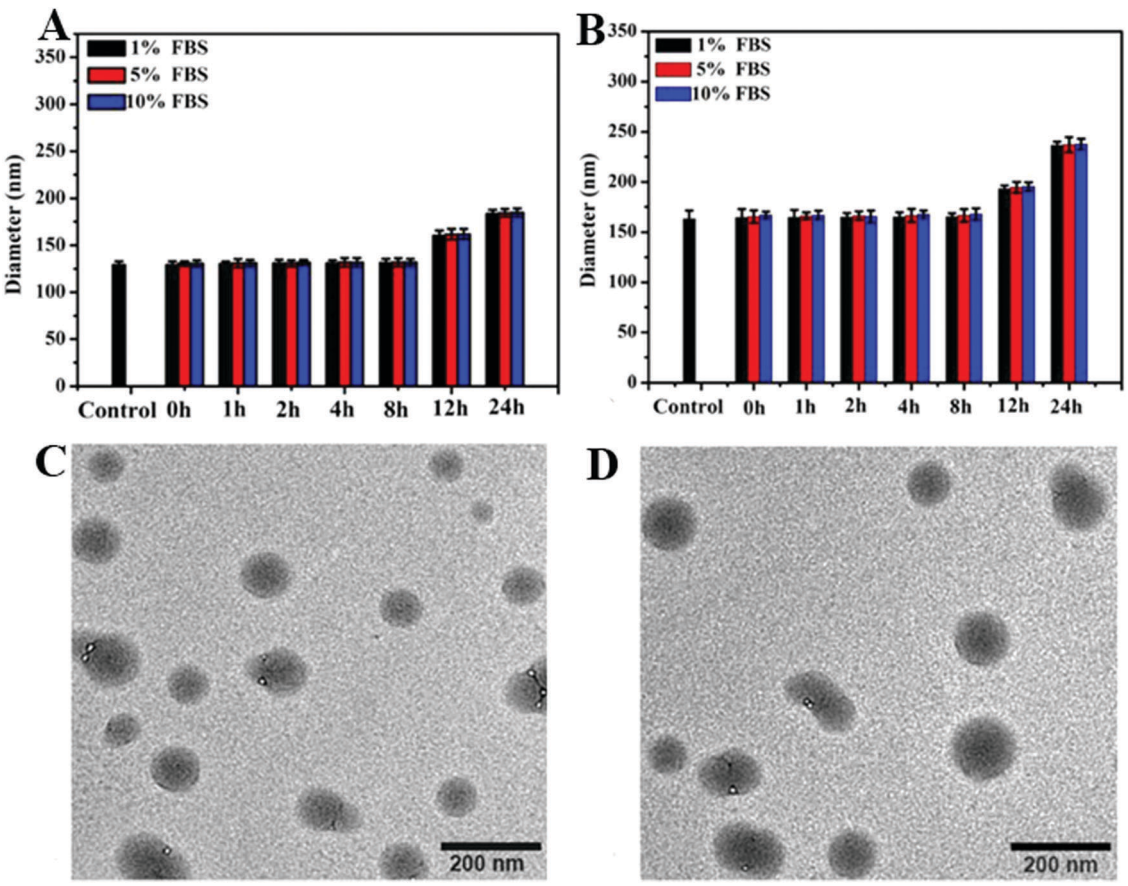

Fig. 3 The dependence of the nanoparticle size on the incubation time in FBS at 37 °C ($PDCB_{30}$, A; $PDCB_{40}$, B) and the TEM photographs ($PDCB_{30}$, C; $PDCB_{40}$, D) for the PDCBs. Data are presented as means ± SD (n = 5).

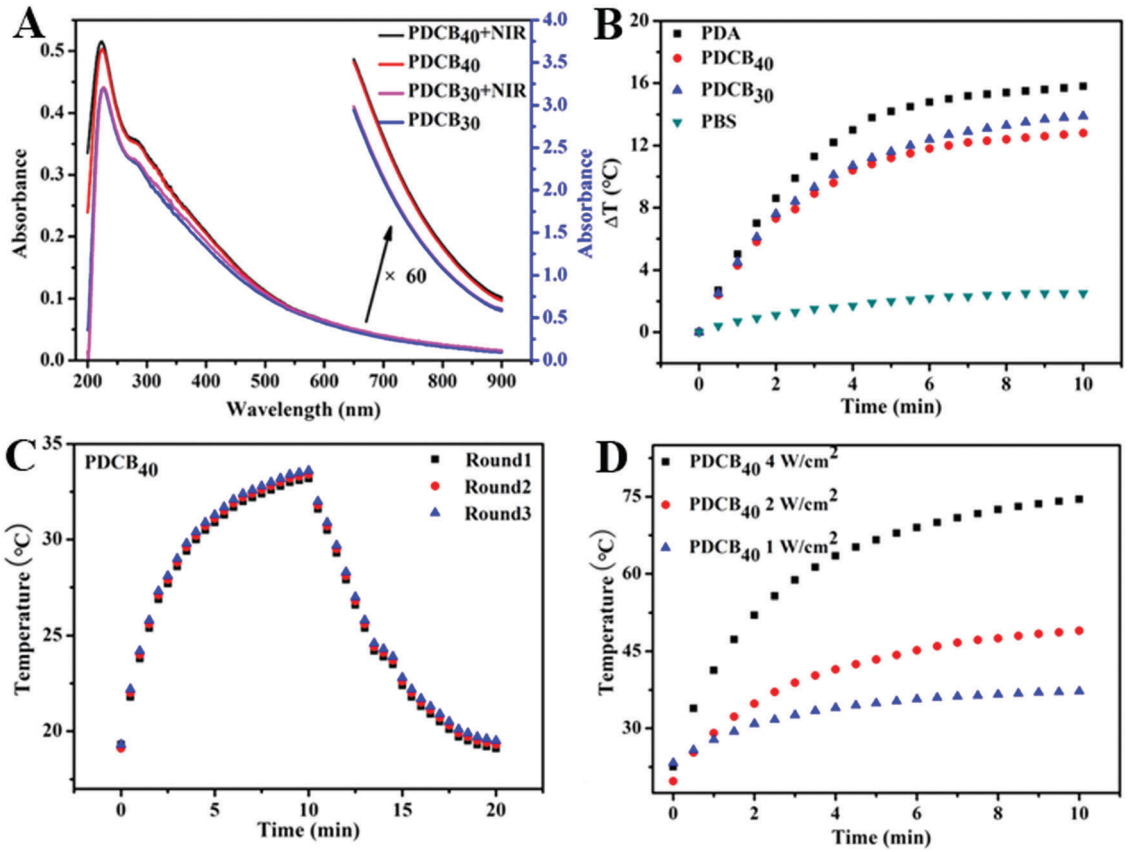

Fig. 4 (A) The UV-Vis-NIR spectra for the PDCBs solutions ($PDCB_{30}$, 500 μg mL^{-1}; $PDCB_{40}$, 400 μg mL^{-1}) or the 60-fold diluted solutions and those under NIR irradiation (808 nm, 1 W cm^{-2}, 10 min). (B) The temperature-elevating magnitude of the PDA (500 μg mL^{-1}) or PDCBs solutions against the irradiation time. (C) The temperature change curves of the $PDCB_{40}$ solution during laser on/off cycles. (D) Heating curves of the $PDCB_{40}$ solution against the irradiation time with different power intensities.

consistent with the UV-Vis-NIR spectra. Furthermore, the ΔT magnitude can be easily tuned using the laser power density and the nanoparticle concentration (Fig. 4D and Fig. S6, ESI†). Notably, both the $PDCB_{30}$ and $PDCB_{40}$ have a higher photothermal conversion efficiency of about 37.2% and 39.1%, which is comparable to 40.3% for pure PDA.[21,24,43] In all, these findings demonstrate that the high drug-loading polyprodrug PDCBs intrinsically possesses a good NIR-absorbing capability, a high photothermal conversion efficiency, and excellent photostability.

Compared to the physically-loaded polymeric nanodrug formulations, the polymer–drug conjugate counterparts can minimize early leaking of the drug into the bloodstream, enhancing the drug efficacy and reducing the side effects.[38–42] The next question to answer is upon various triggers to mimic the intracellular cytosolic reduction (10 mM DTT) and/or acidic endolysosome milieu (pH = 5), do the PDCBs demonstrate an intracellular dual stimuli-sensitive drug release profile? $PDCB_{30}$ and $PDCB_{40}$ (Fig. 5A and B), released about 41–46% of the drug at pH 5.0 for 12 h, while only 3–6% of the drug was found at pH 7.4. Moreover, the mass spectroscopy confirmed that the CB was hydrolyzed at pH 5.0 while no CB was found at pH 7.4 (Fig. S7, ESI†). Upon addition of 10 mM DTT or 10 mM DTT + pH 5.0, the accumulative drug release at 37 °C reached 44% and 94%, respectively. After treatment using 10 mM DTT, the maximal UV absorption of $PDCB_{40}$ red shifted from 225 to 260 nm, which is indicative of the disulfide bond cleavage and production of the CB derivative. These data clearly show that the reduction and the combined stimuli of 10 mM DTT + pH 5.0 triggered an accelerated drug release and a synergistic action, which was caused by the cleavage of the reduction-sensitive disulfide bond and the combined action of the cleavage and the pH-sensitive hydrolysis (Scheme S1, ESI†).[44–46] It should be noted that the DTT trigger mainly produced the adduct of CB with 2,2′-dithiodiethanol while both CB and the adduct were found at 10 mM DTT + pH 5.0.

During the drug release process, the size change of the PDCBs under different triggers was monitored on-line using DLS. When the PDCBs were incubated at pH 5.0 or with 10 mM DTT at 37 °C, they promptly increased to form larger aggregates (about 2–2.5 μm) within about 3 h and then remained stable for 10 h (Fig. 5C and D). This stimuli-sensitive size change of the PDCBs suggests that the hydrophobic CB or its adduct was quickly detached from the nanoparticles owing to the acidic hydrolysis or reduction-triggered cleavage, as monitored using mass spectroscopy (Fig. S7, ESI†). As characterized using TEM (Fig. S8, ESI†), bigger aggregates were formed after the PDCBs were incubated at an acidic pH of 5.0 or after a 10 mM

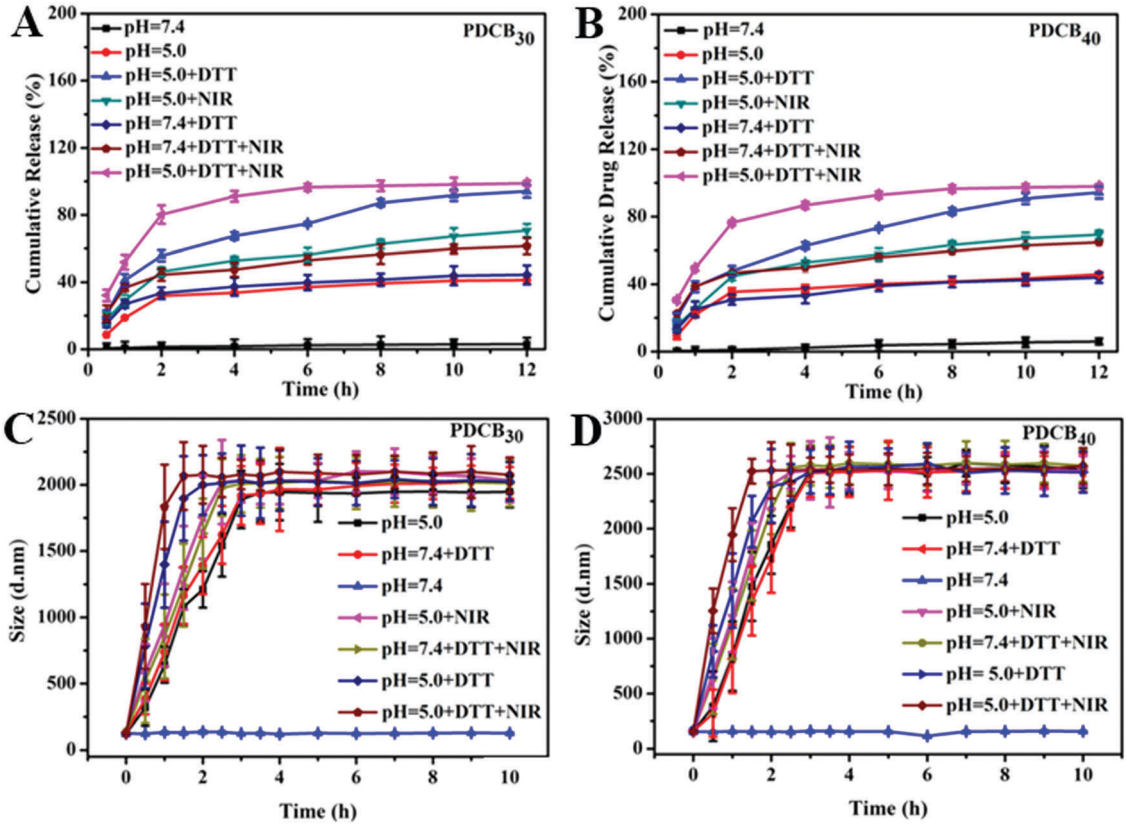

Fig. 5 The pH- and DTT-cleavable and NIR-triggered drug release profiles (A and B), and the DLS size change (C and D) dependent on the time in PBS at 37 °C (n = 6).

DTT reduction. This TEM result is basically consistent with the results of the DLS. The zeta potential measurements showed that the negatively charged nanoparticles of about −30 mV transformed into positively charged nanoparticles of 11.2 mV at pH 5.0, however, they decreased to −43.7 mV at 10 mM DTT. Accordingly, this nanoparticle swelling and aggregation was postulated to occur by two stages: (1) the decreased hydrophobic interaction derived from the CB detachment and the electrostatic repulsion derived from the protonated dopamine moiety ($-NH_3^+$) at pH 5.0, or the decreased negative charge at 10 mM DTT, would swell the original nanoparticles, and (2) the hydrogen-bonding interactions derived from the newly produced 3,4-dihydroxybenzenepropanoic (–COOH) or the thiol-disulfide bond exchanges might connect the swollen nanoparticles to form larger aggregates[37–39] (Scheme S1, ESI†). This detailed mechanism needs further investigation in ongoing work. Upon mild NIR irradiation with a pH 5.0 or 10 mM DTT (*i.e.*, dual triggers), the accumulative drug release in 12 h increased by about 39–71% owing to the photothermal effect which accelerated the drug diffusion from the nanoparticles, inducing a fast drug release.[10–12] Specifically, the triple triggers of pH 5.0 + DTT + NIR achieved the fastest drug release profile with a 76.4% drug release in 2 h compared to the dual triggers of pH 5.0 + DTT, meaning that the mild NIR irradiation sharply enhanced the drug diffusion. Similarly, the dual triggers of pH 5.0 + NIR or pH 7.4 + 10 mM DTT + NIR accelerated the nanoparticles to enlarge and balance at about 2.5 h, while the balancing time reduced to about 2 h and 1.5 h at pH 5.0 + 10 mM DTT and pH 5.0 + 10 mM DTT + NIR, respectively, further verifying the synergistic actions of these dual or triple triggers. It should be noted that the triple stimuli-triggered drug release for the PDCBs was controlled not only by the triggers of pH, DTT, and NIR, but also by the diffusion barrier from the nanoparticles, which could induce a delay in the drug release in accordance with the size change of the nanoparticles.[37,43] Collectively, the polyprodrug PDCBs present intracellular endo-lysosomal pH, cytosolic reduction, and external NIR-triggered drug release profiles, which are expected to synergistically enhance the CT efficacy.

3.3 *In vitro* PT-CT, cellular internalization and trafficking, and *in vivo* pharmacokinetics

Upon mild NIR irradiation (808 nm, 1 W cm^{-2}, 10 min) and/or incubation with PDA for 48 h, all of the L929, HeLa, and MCF-7 cell lines remained alive above 95% (Fig. S9, ESI†). These data show that mild NIR irradiation and PDA itself induce negligible cytotoxicity in the healthy and carcinoma cell lines. Upon mild NIR irradiation and/or with 0.1 mM BSO (as an inhibitor to prohibit the cytosolic synthesis of reductive GSH), both the PDCBS and the free CB were incubated with HeLa and MCF-7 for 48 h, respectively. The drug-induced cytotoxicity of the PDCBs or free CB is dose-dependent and the cell viability gradually decreased with an increase in the PDCB or the drug

concentration under various conditions (Fig. 6). Upon the treatment with 0.1 mM BSO, the IC_{50} of $PDCB_{40}$ greatly increased from 14.03 to 30.28 μg mL^{-1} for the HeLa cells and from 9.72 to 28.11 μg mL^{-1} for the MCF-7 cells; similar results were obtained for $PDCB_{30}$ when incubated with 0.1 mM BSO. BSO reduced the cytosolic GSH concentration, hindering the disulfide bond cleavage in the PDCBs, thus producing an attenuated drug release and an inhibition effect.[45]

Does mild photothermia produce a synergistic action on the polyprodrug release induced CT? Considering the sole photothermal action of the PDA component and the drug-loading capacity, the IC_{50} of the pure PDA nanoparticles (*i.e.*, IC_{50} (PT)) was used to represent the single PT of the PDCBs while the IC_{50} (combination PT) was calculated using the PDA percentage of the PDCBs for the combination PT.[43,48–51] Based on the PDA concentration, both $PDCB_{40}$ and $PDCB_{30}$ gave a IC_{50} of 53.76 μg mL^{-1} (HeLa) or 69.34 μg mL^{-1} (MCF-7) for a single PT (Fig. S10, ESI†). Based on the CB concentration, both the $PDCB_{40}$ and $PDCB_{30}$ gave an IC_{50} of 14.03 μg mL^{-1} (HeLa) or 9.72 μg mL^{-1} (MCF-7) and 14.15 μg mL^{-1} (HeLa) or 9.92 μg mL^{-1} (MCF-7) for a single CT, respectively (Fig. 6). As for the combination PT-CT, $PDCB_{40}$ gave an IC_{50} of 5.23 μg mL^{-1} (HeLa) or 5.23 μg mL^{-1} (MCF-7) for the combination PT and that of 3.69 μg mL^{-1} (HeLa) or 3.49 μg mL^{-1} (MCF-7) for the combination CT; $PDCB_{30}$ showed an IC_{50} of 8.44 μg mL^{-1} (HeLa) or 8.45 μg mL^{-1} (MCF-7) and that of 3.61 μg mL^{-1} (HeLa) or 3.62 μg mL^{-1} (MCF-7) for the combination PT and the combination CT, respectively. The combination index (CI) is generally used to evaluate the synergistic effect between different drugs and/or therapies.[48–51] A CI of less than 1 implies a synergistic effect while a CI greater than 1 or equal to 1 suggest an adverse or additive action; the smaller the CI, the better the different drugs and/or therapies act synergistically. Both the $PDCB_{40}$ and $PDCB_{30}$ gave a low CI of 0.37 (HeLa) or 0.43 (MCF-7) and 0.41 (HeLa) or 0.49 (MCF-7), respectively. That is to say, upon mild NIR irradiation, $PDCB_{40}$ gave a better synergistic effect than $PDCB_{30}$. Thus, the mild PT-CT treatment implemented by both the PDCBs and the mild NIR irradiation both demonstrate an excellent and synergistic antitumor activity for killing HeLa and MCF-7 cell lines.[43,48] Furthermore, this synergistic effect between the hyperthermia and polyprodrug-induced CT has been clarified using the techniques including flow cytometry, fluorescence microscopy, and CLSM.

To provide further insight into the synergistic effect between mild PT and CT, we applied flow cytometry and fluorescence microscopy to study the cellular uptake of the PDCBs in MCF-7. After MCF-7 was incubated with CB, CB + NIR, $PDCB_{40}$, $PDCB_{40}$ + NIR, and $PDCB_{40}$ + BSO at predetermined time intervals, flow cytometry histograms were recorded in Fig. 7 and Fig. S11 (ESI†). Compared to those obtained without mild NIR irradiation,

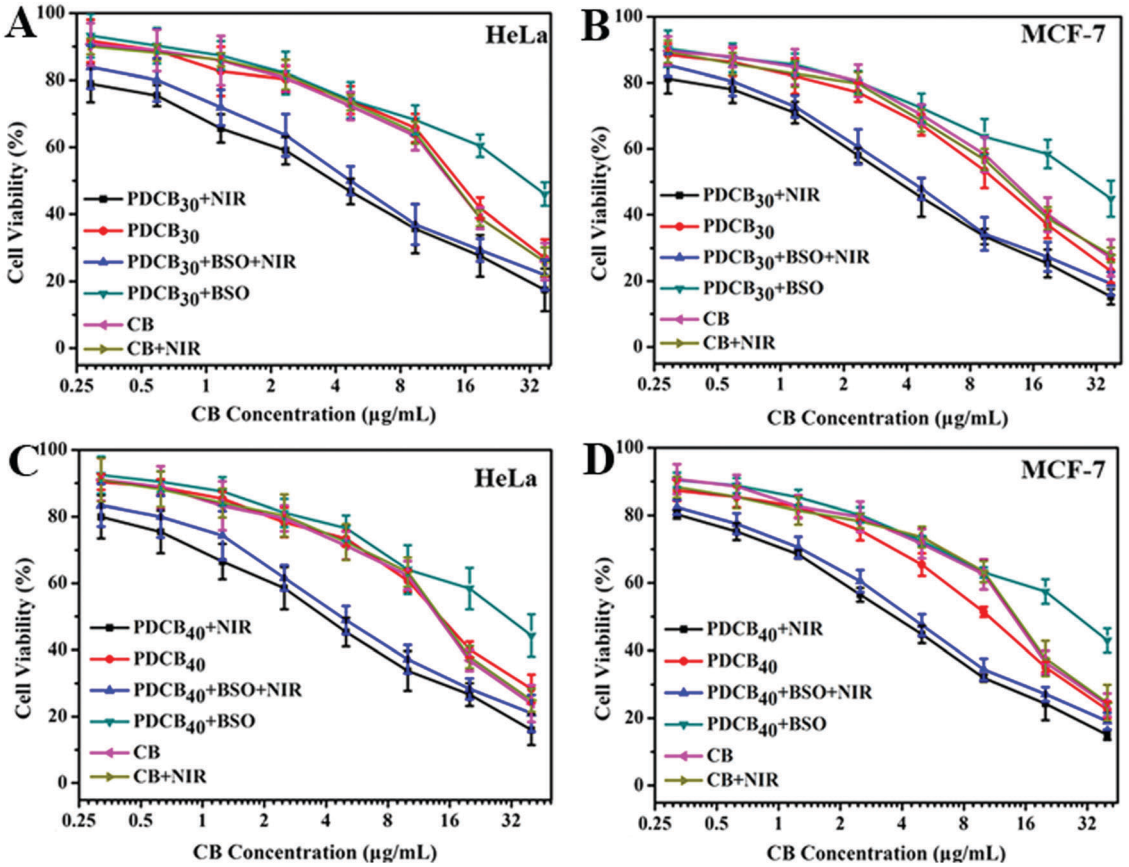

Fig. 6 Cytotoxicity of $PDCB_{30}$ or $PDCB_{40}$ incubated with HeLa (A and C) or MCF-7 (B and D) for 48 h at different conditions. All cell viabilities were tested six times (n = 6).

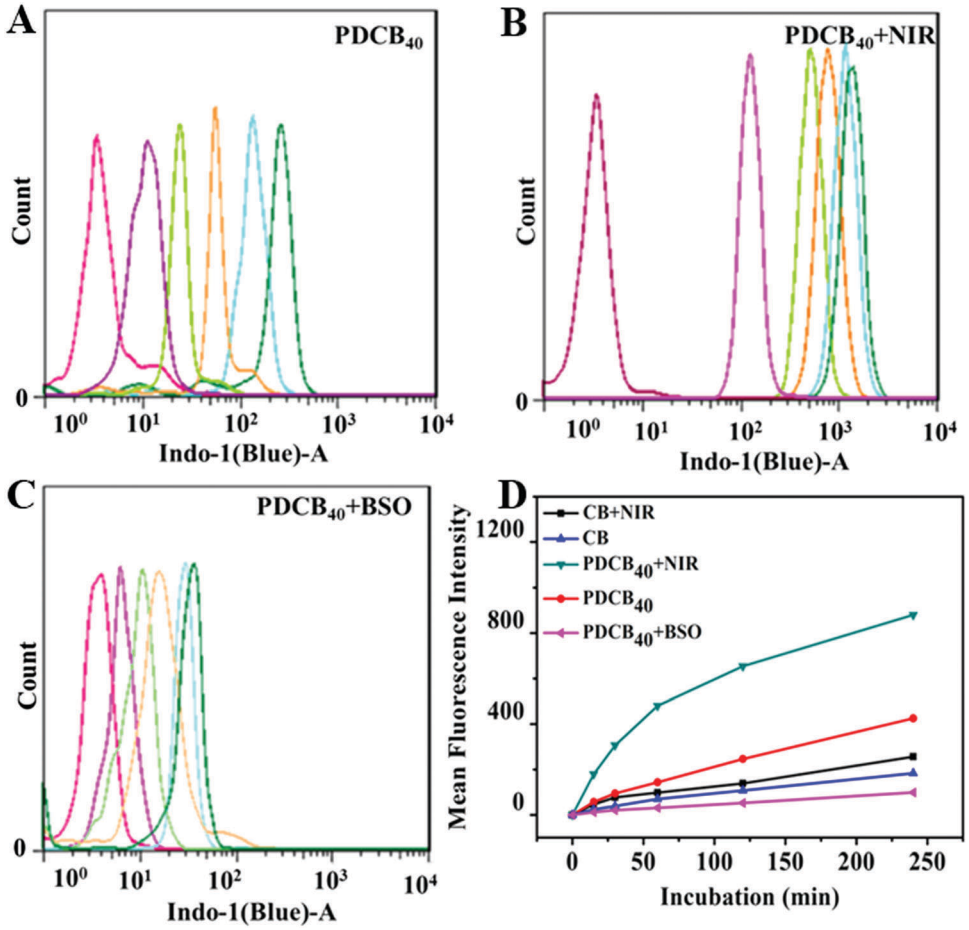

Fig. 7 Flow cytometry histograms (A, B and C) and the time-dependent fluorescence intensity (D) of MCF-7 incubated with $PDCB_{40}$ under different conditions (red, control; purple, 15 min; green, 0.5 h; orange, 1 h; blue, 2 h; and olive, 4 h).

the mean fluorescence intensity of the MCF-7 treated with $PDCB_{40}$ + NIR increased by about 1.1-fold at 4 h, which was about 4.8-fold higher than the control treated with CB. These results indicate that the $PDCB_{40}$ was more efficiently taken up by the MCF-7 compared to CB, and the mild NIR irradiation could further facilitate the cellular uptake owing to the photothermally enhanced membrane permeability.[43,48] This large difference in the cellular uptake for CB and $PDCB_{40}$ is because $PDCB_{40}$, with a diameter of <200 nm, was probably internalized by MCF-7 *via* an energy-mediated endocytosis process compared to the passive diffusion path adopted for the CB.

As observed using fluorescence microscopy (Fig. S12, ESI†), the MCF-7 cells incubated with $PDCB_{40}$ showed a time-dependent fluorescence intensity upon mild NIR irradiation or introduction of the BSO inhibitor, which is consistent with the above-discussed flow cytometry results. Moreover, the MCF-7 cells treated with $PDCB_{40}$ + NIR showed the strongest pink fluorescence (the merged color of both the blue fluorescence emitted from the CB and the red fluorescence emitted from the PI) in the PI-stained nuclei at 4 h compared to those without NIR irradiation or with BSO or with free CB. This PI-staining observation further supports the above findings, as monitored using flow cytometry.

Efficient cell internalization and subsequent intracellular trafficking would greatly improve the CT.[35–37] Does photothermia enhance the ability of the nanoparticles to escape the endolysosome? After the MCF-7 cells were incubated with $PDCB_{40}$ (CB emits blue fluorescence) for 2 h with/without NIR irradiation, the endolysosomes and the nuclei were counterstained using LysoTracker (green) and PI (red) and observed using CLSM (Fig. 8A and B and Fig. S13, ESI†). Without the NIR irradiation, $PDCB_{40}$ was observed to mainly enter into endolysosomes owing to the colocalization of the blue and green fluorescence. Upon mild NIR irradiation, however, a merged blue and red fluorescence (*i.e.*, a pink color) was clearly observed, which suggests that more PDCBs escaped from the endolysosome into the cytoplasm, along with the many released CB molecules that entered into the nuclei.[52–56] The MCF-7 cells treated with $PDCB_{40}$ + NIR irradiation showed a lower colocalization value of $(16.6 \pm 6.5)\%$, revealing the NIR-triggered higher endolysosomal disruption and greater escape capability of $PDCB_{40}$ compared with that of $(72.4 \pm 5.7)\%$ without NIR irradiation. These results demonstrated that $PDCB_{40}$ was rapidly trafficked from the endolysosomes under NIR irradiation owing to the hyperthermia induced endolysosomal membrane disruption and instability.[52–56] Collectively, the above findings clarified that

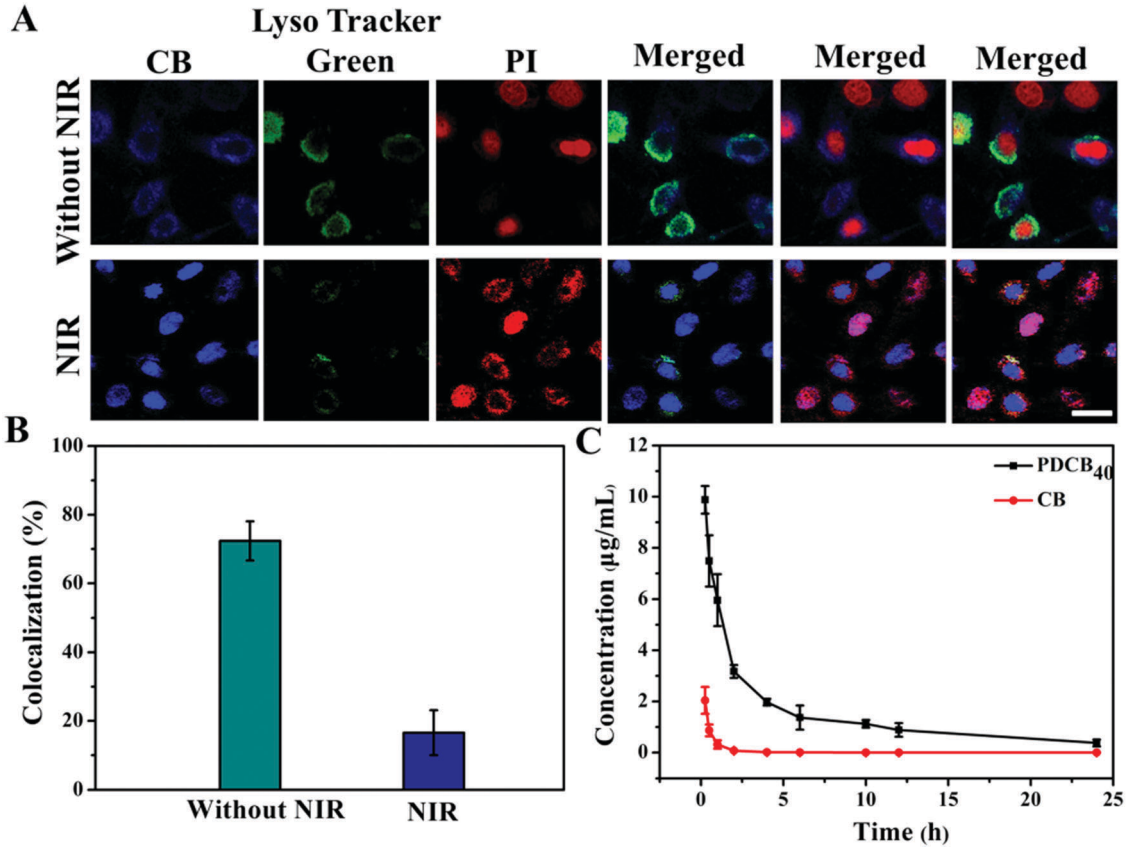

Fig. 8 (A) CLSM photographs for the intracellular distribution of $PDCB_{40}$ incubated with MCF-7 for 2 h with/without NIR irradiation, the scale bar represents 25 μm. (B) Quantification of the co-localization between $PDCB_{40}$ and LysoTracker (n = 15). (C) *In vivo* pharmacokinetics curves for $PDCB_{40}$ and CB (n = 4).

mild NIR irradiation could facilitate cellular internalization and the subcellular trafficking of $PDCB_{40}$, generating a synergistic effect between the CT and PT at the cellular level, as verified by MTT, flow cytometry, fluorescence microscopy, and CLSM.

As $PDCB_{40}$ has a higher CB-loading, better antitumor activity and a smaller CI than $PDCB_{30}$, the *in vivo* performance was evaluated using $PDCB_{40}$ as an example. Following intravenous injections in SD mice and the collection of blood samples at various predetermined times, the pharmacokinetic profiles of $PDCB_{40}$ (8 mg kg^{-1} CB equiv.) and the control of the free CB were recorded in Fig. 8C. As expected, free CB was rapidly cleared from the plasma, whereas $PDCB_{40}$ achieved a higher bloodstream CB concentration and a longer elimination half-life time ($t_{1/2\beta}$) of (1.34 ± 0.17) h, which is about 3.62-fold greater than that found for free CB, (0.37 ± 0.04) h. Moreover, the area under the curve (AUC) for $PDCB_{40}$ was 33.12 ± 0.85 mg h L^{-1} and this is about 33.8-fold greater than 0.98 ± 0.02 mg h L^{-1} found for free CB. In all, the polyprodrug nanoparticle formulation of $PDCB_{40}$ obviously prolongs the blood circulation time of CB owing to the dual nanoscale and prodrug attributes, which are expected to be physiologically stable allowing an efficient CT to be attained *in vivo*.[37–42]

3.4 *In vivo* biodistribution and photo-mediated imaging

Precise and efficacious cancer therapy using nanoparticles depends on several barrier steps, and the EPR, in which the nanoparticles passively accumulate and penetrate into tumor site, plays a decisive role in addition to the aforementioned long blood circulation of the non-leaking polyprodrug nanoparticles.[57] The anticancer drug doxorubicin (DOX) emits a strong red fluorescence and the physically DOX-loaded nanoparticles with minimal drug leakage can be facilely used to monitor *in vivo* tissue biodistribution using a small animal fluorescent imaging system.[58–61] Utilizing strong π–π stacking and hydrogen-bonding interactions between the PDA network and the DOX, a certain amount of DOX (52.6 wt%) was physically absorbed onto $PDCB_{40}$ to form DOX-loaded $PDCB_{40}$; meanwhile minimal premature DOX leakage was exhibited in PBS at 37 °C, inducing a reduced effect on the *in vivo* biodistribution.[30,62] Free DOX and DOX-loaded $PDCB_{40}$ (5.3 mg kg^{-1} DOX equiv.) were intravenously injected *via* the tail vein into MCF-7 tumor-bearing nude mice. As shown in Fig. 9A, the fluorescence signal for the mice treated with DOX-loaded $PDCB_{40}$ progressively increased in the tumor site, and was strongest at 10 h, it then grew weaker, but was still observable at 24 h; on the other hand, the mice treated with free DOX quickly attained the strongest signal at 6 h and this sharply attenuated and was negligible at 24 h. These data indicate that the DOX-loaded $PDCB_{40}$ formulation facilitated fluorescent imaging owing to the EPR effect and enabled a longer blood retention time, while free DOX was quickly cleared from the bloodstream.[58–61]

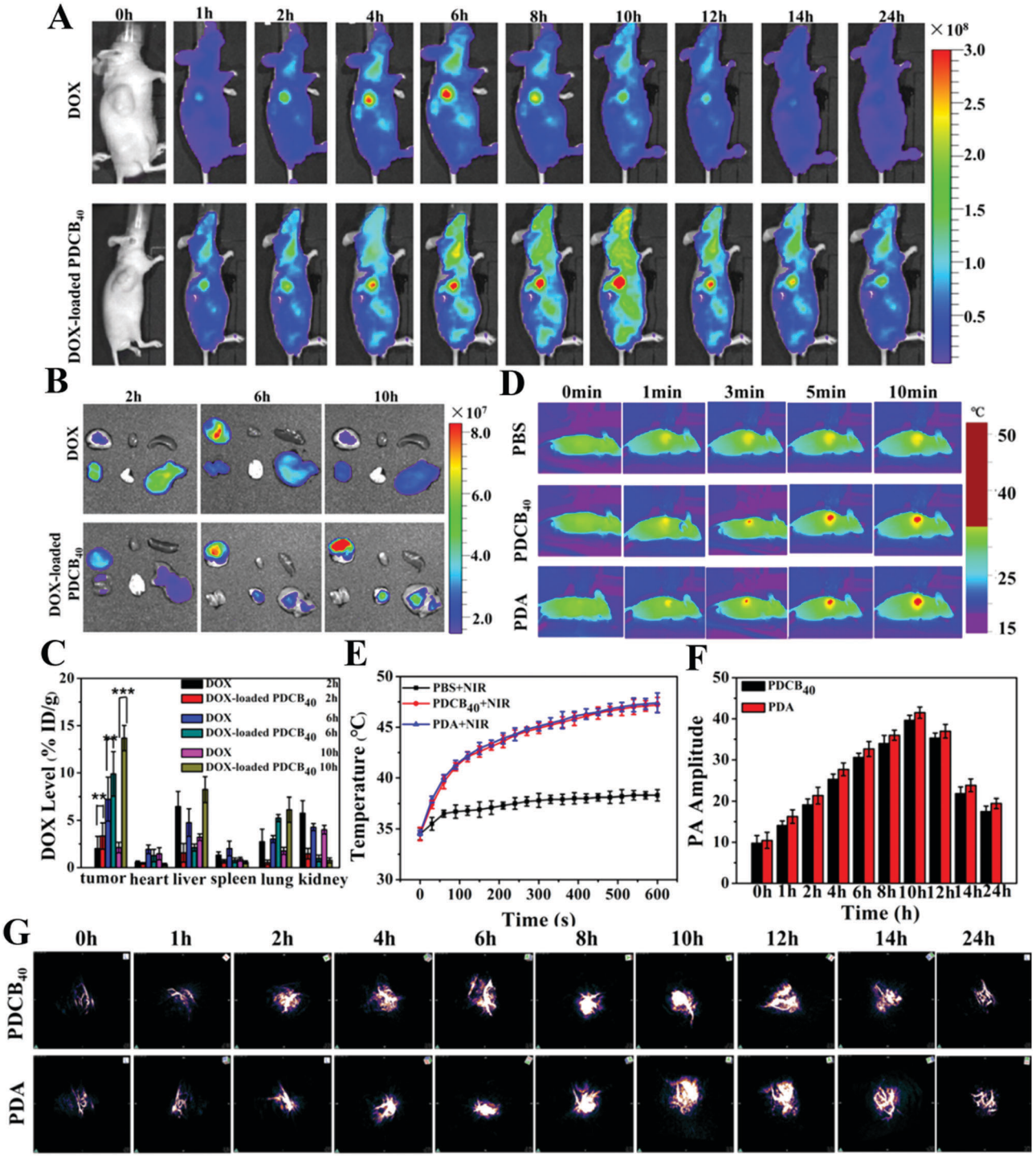

Fig. 9 (A) *In vivo* fluorescent imaging of the tumor-bearing nude mice after intravenous injection of DOX or DOX-loaded $PDCB_{40}$. (B) *Ex vivo* imaging of the major organs and the tumors. (C) Biodistribution of DOX in different tissues at a dosage of 5.3 mg kg^{-1}. The data are shown as mean ± SD (n = 3); (**) indicates $P < 0.01$, (***) indicates $P < 0.001$. (D) Photothermal imaging of the mice upon mild NIR irradiation. (E) The temperature evolution curve of the tumor site over the irradiation time (n = 4). (F) The PA signal intensity of the tumor over time following intravenous injection of PDA or $PDCB_{40}$ at same dose (n = 3). (G) The 3D PA images of the tumor at different time intervals.

To investigate the amount of $PDCB_{40}$ in the tumor and other major organs *ex vivo* (the heart, liver, spleen, lung, and kidneys), all mice were sacrificed after intravenous injection at different time intervals (2, 6 and 10 h). For the mice treated with DOX-loaded $PDCB_{40}$, the DOX fluorescence in the tumor site was at its strongest at 10 h compared to the other major organs, suggesting a selective accumulation of $PDCB_{40}$ in the tumor (Fig. 9B). Considering the DOX level (% ID/g) in the tumor site,

the mice treated with DOX-loaded $PDCB_{40}$ showed a 6.5-fold greater level DOX at 10 h compared to those used as the control and treated with free DOX (Fig. 9C). These *in vivo* and *ex vivo* data show that the polyprodrug $PDCB_{40}$ formulation indeed has a selective tumor accumulation effect.[43,58–61]

Next, we evaluated the *in vivo* photothermal effect and the imaging of $PDCB_{40}$. Three groups of MCF-7 tumor-bearing mice were intravenously administrated with PBS, PDA and $PDCB_{40}$ at a time point of 0 day, respectively. At 10 h after the injection and after mild NIR irradiation (808 nm, 1 W cm^{-2}, 10 min),

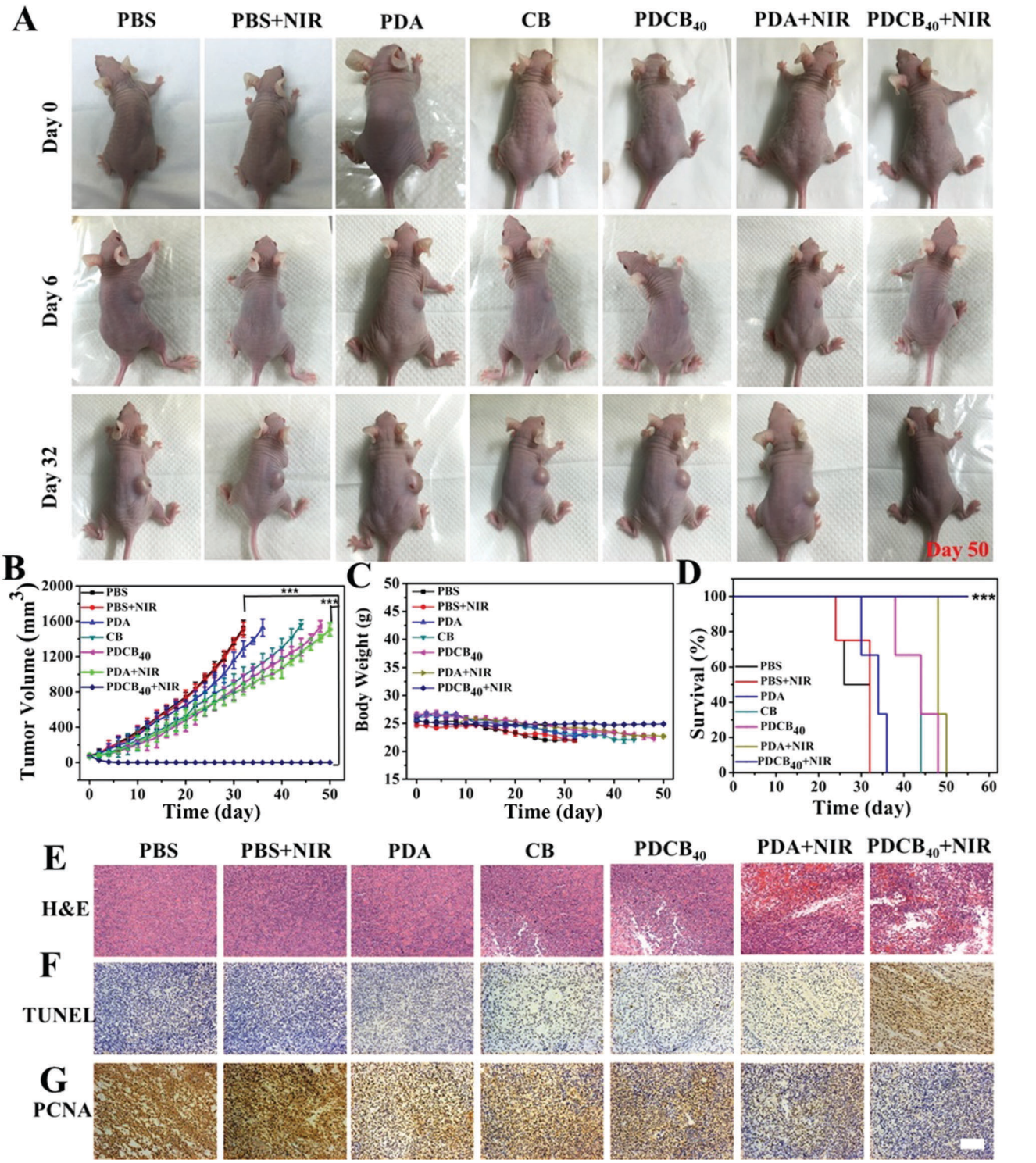

Fig. 10 (A) Photographs of the mice undergoing various treatments. The dependence of the tumor volume (B) or body weight (C) of the mice on time. (D) Survival curve of the mice with various treatments (n = 4); (***) indicates $P < 0.001$. H&E stained images (E), TUNEL (F), and PCNA (G) of the dissected tumors after 32 days of treatment and the healed tissue for the $PDCB_{40}$ + NIR group, the scale bar represents 150 μm.

the tumor-sites of the three groups were monitored on-line using a thermal imaging camera during the irradiation process. As shown in Fig. 9D and E, the tumor-site temperature of the mice treated with PDA or $PDCB_{40}$ increased to about 45 °C from 34.5 °C after 5 min of NIR irradiation, and then slowly heated up to about 47 °C; in contrast, the PBS group only increased by about 3.8 °C. It should be note that $PDCB_{40}$ + NIR can elevate the tumor-site temperature to over 43 °C in 3 min and then kill the cancer cells from 3 to 10 min as cancer cells are vulnerable to hyperthermia above 43 °C.[63] These data convincingly demonstrate that $PDCB_{40}$ can mediate a mild photothermic effect on the tumor upon mild NIR irradiation.

As an emerging noninvasive imaging modality, photoacoustic (PA) imaging is attractive for cancer imaging and diagnosis as both nanoparticles and NIR irradiation result in heat fluctuations and ultrasonic waves, making 2D or 3D imaging possible in a target containing accumulated nanoparticles.[31,32,43,64] For the PDA (control) and $PDCB_{40}$ treated mice (Fig. 9G and F), the PA signal of the tumor site enhanced progressively and reached a maximum at 10 h post injection. For the $PDCB_{40}$ treated mice, the strongest PA signal at 10 h was 4.1-fold higher than that of the contrast image at 0 h, although this was a little attenuated (4.5%) compared with the control PDA; then the PA signal gradually reduced but remained 1.8-fold stronger than the contrast image at 24 h. These findings indicate that $PDCB_{40}$ has an intrinsic and excellent PA imaging ability *in vivo* owing to a selective accumulation and retention effect in the tumor site. It should be noted that the PDA-mediated photoacoustic imaging result was consistent with the above mentioned DOX-induced fluorescent imaging results when utilizing the DOX-loaded $PDCB_{40}$. Collectively, the NIR-absorbing $PDCB_{40}$ intrinsically possesses both photothermal and PA imaging modalities, making it useful as a novel nanotheranostic agent for imaging-guided precision cancer therapy.[35–37]

3.5 *In vivo* antitumor activity, H&E, TUNEL and PCNA assays

Based on the *in vitro* and *in vivo* studies of $PDCB_{40}$, we comparatively examined the antitumor performance of $PDCB_{40}$ by using MCF-7-bearing nude mice with an average tumor volume of 60–80 mm^3. On day 0, the mice were placed into seven groups and intravenously administrated with either PBS, PBS + NIR, PDA, free CB (8 mg kg^{-1}), PDA + NIR (PT), $PDCB_{40}$ (CT, 8 mg CB equiv. per kg), or $PDCB_{40}$ + NIR (PT + CT), respectively. Note that all the groups were injected once on day 0 with/without one dose of NIR-irradiation (808 nm, 1 W cm^{-2}, 10 min). As shown in Fig. 10A, the tumors in mice treated with the PT-CT group completely regressed without skin scarring or burning damage on day 6, and did not recur over the 50 day evaluation period. However, the tumors of those from the single CT and PT groups increased continuously although their tumor growth rates were lower than those in the PBS, PBS + NIR, PDA, and free CB groups (Fig. 10B and Fig. S14, ESI†). Specifically, compared to the PBS group, the mild PT-CT treatment achieved a tumor inhibitory rate (TIR) of 100%, which is significantly higher than that of free CB (35.5 ± 7.3%), CT (41.1 ± 8.3%), and mild PT (45.4 ± 5.3%). During the survival study, no mice in the PBS, PBS + NIR, PDA groups remained alive on days 32–36 owing to the oversized tumors (> 1500 mm^3), whereas none of single CT and single PT groups were surviving on day 50 (Fig. 10D). Impressively, all of the mice in the PT + CT group remained alive with complete and traceless tumor ablation on 50 day after one injection and one mild dose of NIR irradiation; however, heavy scar and skin burning damage were often observed in the normal PT and PT-CT groups at more than 50 °C upon a high intensity or high dose of NIR irradiation.[17–20] These findings convincingly demonstrate that the mild PT-CT treatment produced a superior and synergetic therapeutic efficacy *in vivo*. In addition, all mice in the PT-CT group showed little change in their mean weight during the 50 days compared with the other groups, suggesting minimal systematic toxicity of $PDCB_{40}$ under mild NIR irradiation (Fig. 10C).

To further assess the antitumor efficacy of the above treatments, the dissected tumors and major organs (liver, kidneys, spleen, lung and heart) of all of the groups on day 32 were stained using H&E for histological analysis. Heavily decreased cellularity, and nuclear shrinkage and fragmentation were observed for the completely-healed tissue (*i.e.*, original tumor site) in the mild PT-CT group compared to the tumors from the free CB, mild PT, and CT groups (Fig. 10E). The main organs for all of the mice from the three therapeutic groups (PT, CT, and PT + CT) and the three control groups (PBS, PBS + NIR, PDA) showed no obvious pathological change and damage, although the kidneys from the mice in the free CB group changed slightly (Fig. S15, ESI†). Moreover, both the tumor cell apoptosis and proliferation were examined using TUNEL and PCNA, respectively. The mild PT + CT group presented a significant cell apoptosis compared to a moderate level in the mild PT, CT and free CB groups, a small amount was observed in the PDA group, and a minimal amount was found in the PBS and PBS + NIR groups (Fig. 10F). On the contrary, the PCNA-positive tumor cells were reduced the most in the mice from the mild PT + CT group, with the next most reduced in the mild PT, CT and free CB groups, less in the PDA group, and the least in the PBS and PBS + NIR groups (Fig. 10G). In all, by one intravenous injection and one mild dose of NIR irradiation, the polyprodrug formulation of $PDCB_{40}$ generated a superior and synergistic antitumor efficacy *in vivo* and achieved complete and traceless ablation of solid tumors without recurrence in 50 days, providing a mild PT-CT treatment that is practical for tumor therapy.[43,46,63–69]

4. Conclusions

To address the key dilemmas and enhance the transition potential of cancer PT and PT-CT treatments, we put forward an innovative strategy to leverage the hyperthermia and high drug-loading capacity of a polyprodrug to achieve mild PT-CT treatment. We have rationally constructed a novel class of PDCBs conjugate nanotheranostics, which present good photothermal properties, have intracellular pH-, reduction-cleavable, and NIR-triggered drug release profiles, and demonstrate a

prolonged blood circulation time and selective tumor accumulation effect. By monitoring the treatments using MTT, flow cytometry, fluorescence microscopy, and CLSM, it was shown that $PDCB_{40}$ + mild NIR irradiation could efficiently promote cellular internalization and subcellular trafficking, producing an excellent and synergistic antitumor effect *in vitro*. In addition to exhibiting good photothermal and photoacoustic imaging capabilities, the polyprodrug $PDCB_{40}$ formulation produced superior antitumor efficacy using one intravenous injection and a single mild dose of NIR irradiation, achieving complete and traceless ablation of a solid MCF-7 tumor without recurrence within 50 days. Significantly, this work opens up a new avenue for the development of a polyprodrug-based mild PT-CT treatment that allows intrinsic photothermal and photoacoustic imaging for practical and precise cancer therapy.

Conflicts of interest

There are no conflicts to declare.

Acknowledgements

C. M. DONG thanks the National Natural Science Foundation of China (21774074 & 21474061). Financial support from the Innovation Program of Shanghai Municipal Education Commission (201701070002E0061) and the Innovation Fund (IFPM2016B004) of Shanghai Jiao Tong University & Affiliated Sixth People's Hospital South Campus are also appreciated.

References

1 H. S. Jung, P. Verwilst, A. Sharma, J. Shin, J. L. Sessler and J. S. Kim, *Chem. Soc. Rev.*, 2018, **47**, 2280–2297.
2 M. Karimi, P. S. Zangabad, S. Baghaee-Ravari, M. Ghazadeh, H. Mirshekari and M. R. Hamblin, *J. Am. Chem. Soc.*, 2017, **139**, 4584–4610.
3 R. Batul, T. Tamanna, A. Khaliq and A. Yu, *Biomater. Sci.*, 2017, **5**, 1204–1229.
4 M. Abbas, Q. Zou, S. Li and X. Yan, *Adv. Mater.*, 2017, **29**, 1605021.
5 X. Huang, W. Zhang, G. Guan, G. Song, R. Zou and J. Hu, *Acc. Chem. Res.*, 2017, **50**, 2529–2538.
6 C. Liang, L. Xu, G. Song and Z. Liu, *Chem. Soc. Rev.*, 2016, **45**, 6250–6269.
7 Y. Chen, L. Wang and J. Shi, *Nano Today*, 2016, **11**, 292–308.
8 K. K. Ng and G. Zheng, *Chem. Rev.*, 2015, **115**, 11012–11042.
9 J. B. Song, P. Huang, H. W. Duan and X. Y. Chen, *Acc. Chem. Res.*, 2015, **48**, 2506–2515.
10 L. Cheng, C. Wang, L. Feng, K. Yang and Z. Liu, *Chem. Rev.*, 2014, **114**, 10869–10939.
11 V. Shanmugam, S. Selvakumar and C.-S. Yeh, *Chem. Soc. Rev.*, 2014, **43**, 6254–6287.
12 Z. Zhang, J. Wang and C. Y. Chen, *Adv. Mater.*, 2013, **25**, 3869–3880.
13 S. Zhang, H. Chen, G. Zhang, X. Kong, S. Yin, B. Li and L. Wu, *J. Mater. Chem. B*, 2018, **6**, 241–248.
14 T. Wang, D. Wang, H. Yu, M. Wang, J. Liu, B. Feng, F. Zhou, Q. Yin, Z. Zhang, Y. Huang and Y. Li, *ACS Nano*, 2016, **10**, 3496–3508.
15 J. Nam, S. Son, L. J. Ochyl, R. Kuai, A. Schwendeman and J. J. Moon, *Nat. Commun.*, 2018, **9**, 1074.
16 L. Zhang, Y. Qin, Z. Zhang, F. Fan, C. Huang, L. Lu, H. Wang, X. Jin, H. Zhao, D. Kong, C. Wang, H. Sun, X. Leng and D. Zhu, *Acta Biomater.*, 2018, **75**, 371–385.
17 X. Zhen, C. Xie and K. Pu, *Angew. Chem., Int. Ed.*, 2018, **130**, 4002–4006.
18 L. Pan, J. Liu and J. Shi, *ACS Appl. Mater. Interfaces*, 2017, **9**, 15952–15961.
19 Y. Yang, W. Zhu, Z. Dong, Y. Chao, L. Xu, M. Chen and Z. Liu, *Adv. Mater.*, 2017, **29**, 1703588.
20 R. Zhu, F. Gao, J.-G. Piao and L. Yang, *Biomater. Sci.*, 2017, **5**, 1596–1602.
21 R. Mrowczynski, *ACS Appl. Mater. Interfaces*, 2018, **10**, 7541–7561.
22 M. Y. Liu, G. J. Zeng, K. Wang, Q. Wan, L. Tao, X. Y. Zhang and Y. Wei, *Nanoscale*, 2016, **8**, 16819–16840.
23 X. P. Chen, Y. S. Huang, G. Yang, J. X. Li, T. T. Wang, O. H. Schulz and L. K. Jennings, *Curr. Pharm. Des.*, 2015, **21**, 4262–4275.
24 Y. Liu, K. Ai and L. Lu, *Chem. Rev.*, 2014, **114**, 5057–5115.
25 M. D'Ischia, A. Napolitano, V. Ball, C. T. Chen and M. J. Buehler, *Acc. Chem. Res.*, 2014, **47**, 3541–3550.
26 Y. Li, C. Jiang, D. Zhang, Y. Wang, X. Ren, K. Ai, X. Chen and L. Lu, *Acta Biomater.*, 2017, **47**, 124–134.
27 S. H. Kim, I. In and S. Y. Park, *Biomacromolecules*, 2017, **18**, 1825–1835.
28 L. Zhang, H. Su, J. Cai, D. Cheng, Y. Ma, J. Zhang, C. Zhou, S. Liu, H. Shi, Y. Zhang and C. Zhang, *ACS Nano*, 2016, **10**, 10404–10417.
29 X. Wu, L. Zhou, Y. Su and C. M. Dong, *J. Mater. Chem. B*, 2016, **4**, 2142–2152.
30 X. Wang, J. Zhang, Y. Wang, C. Wang, J. Xiao, Q. Zhang and Y. Cheng, *Biomaterials*, 2016, **81**, 114–124.
31 J. Lin, M. Wang, H. Hu, X. Y. Yang, B. Wen, Z. T. Wang, O. Jacobson, J. B. Song, G. F. Zhang, G. Niu, P. Huang and X. Y. Chen, *Adv. Mater.*, 2016, **28**, 3273–3279.
32 Q. Fan, K. Cheng, X. Hu, X. Ma, R. Zhang, M. Yang, X. Lu, L. Xing, W. Huang, S. S. Gambhir and Z. Cheng, *J. Am. Chem. Soc.*, 2014, **136**, 15185–15194.
33 J. Park, T. F. Brust, H. J. Lee, S. C. Lee, V. J. Watts and Y. Yeo, *ACS Nano*, 2014, **8**, 3347–3356.
34 M. Zhang, X. Chen, L. Zhang, L. Li, Z.-M. Su and C. Wang, *Chem. Mater.*, 2018, **30**, 3722–3733.
35 J. Shi, P. W. Kantoff, R. Wooster and O. C. Farokhzad, *Nat. Rev. Cancer*, 2017, **17**, 20–37.
36 Y. Yan, M. Björnmalm and F. Caruso, *ACS Nano*, 2017, **3**, 9512–9517.
37 M. Elsabahy, G. S. Heo, S.-M. Lim, G. Sun and K. L. Wooley, *Chem. Rev.*, 2015, **115**, 10967–11011.
38 X. Pang, Y. Jiang, Q. Xiao, A. W. Leung, H. Hua and C. Xu, *J. Controlled Release*, 2016, **222**, 116–129.

39 R. Tong, L. Tang, L. Ma, R. Baumgartner and J. Cheng, *Chem. Soc. Rev.*, 2014, **43**, 6982–7012.
40 R. Duncan, *J. Controlled Release*, 2014, **190**, 371–380.
41 J. Kopeček, *Adv. Drug Delivery Rev.*, 2013, **65**, 49–59.
42 Y. Hou, Y. Zhou, H. Wang, R. Wang, J. Yuan, Y. Hu, K. Sheng, J. Feng, S. Yang and H. Lu, *J. Am. Chem. Soc.*, 2018, **140**, 1170–1178.
43 C. Du, J. Qian, L. Zhou, Y. Su, R. Zhang and C. M. Dong, *ACS Appl. Mater. Interfaces*, 2017, **9**, 31576–31588.
44 Y. Han, J. Li, M. Zan, S. Luo, Z. Ge and S. Liu, *Polym. Chem.*, 2014, **5**, 3707–3718.
45 S. Lv, Z. Tang, D. Zhang, W. Song, M. Li, J. Lin, H. Liu and X. Chen, *J. Controlled Release*, 2014, **194**, 220–227.
46 Y. Zhang, D. Yang, H. Chen, W. Q. Lim, F. S. Z. Phua, G. An, P. Yang and Y. Zhao, *Biomaterials*, 2018, **163**, 14–24.
47 Q. Wei, K. Achazi, H. Liebe, A. Schulz, P.-L. Michael Noeske, I. Grunwald and R. Haag, *Angew. Chem., Int. Ed.*, 2014, **53**, 11650–11655.
48 X. J. Wu, L. Z. Zhou, Y. Su and C. M. Dong, *Biomacromolecules*, 2016, **17**, 489–2501.
49 Q. Y. Hu, W. J. Sun, C. Wang and Z. Gu, *Adv. Drug Delivery Rev.*, 2016, **98**, 19–34.
50 S. Mignani, M. Bryszewska, B. Klajnert-Maculewicz, M. Zablocka and J.-P. Majoral, *Biomacromolecules*, 2015, **16**, 1–27.
51 L. Ma, M. Kohli and A. Smith, *ACS Nano*, 2013, **7**, 9518–9525.
52 J. Kim, H. Kim and W. J. Kim, *Small*, 2016, **12**, 1184–1192.
53 T.-Y. Hsieh, W.-C. Huang, Y.-D. Kang, C.-Y. Chu, W.-L. Liao, Y.-Y. Chen and S.-Y. Chen, *Adv. Healthcare Mater.*, 2016, **5**, 3016–3026.
54 D. Li, M. Zhang, F. Xu, Y. Chen, B. Chen, Y. Chang, H. Zhong, H. Jin and Y. Huang, *Acta Pharm. Sin. B*, 2018, **8**, 74–84.
55 W. Tao, X. Zhu, X. Yu, X. Zeng, Q. Xiao, X. Zhang, X. Ji, X. Wang, J. Shi, H. Zhang and L. Mei, *Adv. Mater.*, 2017, **29**, 1603276.
56 J. Zhang, X. Zhang, G. Liu, D. Chang, X. Liang, X. Zhu, W. Tao and L. Mei, *Theranostics*, 2016, **6**, 2099–2113.
57 H. Maeda, H. Nakamura and J. Fang, *Adv. Drug Delivery Rev.*, 2013, **65**, 71–79.
58 Y. Zhu, J. Zhang, F. Meng, C. Deng, R. Cheng, J. Feijen and Z. Zhong, *J. Controlled Release*, 2016, **233**, 29–38.
59 D. Li, Z. Tang, Y. Gao, H. Sun and S. Zhou, *Adv. Funct. Mater.*, 2016, **26**, 66–79.
60 L. Wang, Y. Yuan, S. Lin, J. Huang, J. Dai, Q. Jiang, D. Cheng and X. Shuai, *Biomaterials*, 2016, **78**, 40–49.
61 S.-M. Lee, H. Park and K.-H. Yoo, *Adv. Mater.*, 2010, **22**, 4049–4053.
62 Y. Gao, X. Wu, L. Zhou, Y. Su and C. M. Dong, *Macromol. Rapid Commun.*, 2015, **36**, 916–922.
63 J. O. You, P. Guo and D. T. Auguste, *Angew. Chem., Int. Ed.*, 2013, **52**, 4141–4146.
64 J. Yang, S. Zhai, H. Qin, H. Yan, D. Xing and X. Hu, *Biomaterials*, 2018, **176**, 1–12.
65 Y. Chen, H. Li, Y. Deng, H. Sun, X. Ke and T. Ci, *Acta Biomater.*, 2017, **51**, 374–392.
66 Y. Zhang, C. Teh, M. Li, C. Y. Ang, S. Y. Tan, Q. Qu, V. Korzh and Y. Zhao, *Chem. Mater.*, 2016, **28**, 7039–7050.
67 X. Li, M. Takashima, E. Yuba, A. Harada and K. Kono, *Biomaterials*, 2014, **35**, 6576–6584.
68 N. Larson, A. Gormley, N. Frazier and H. Ghandehari, *J. Controlled Release*, 2013, **170**, 41–50.
69 C. Q. Luo, Y. X. Zhou, T. J. Zhou, L. Xing, P. F. Cui, M. Sun, L. Jin, N. Lu and H. L. Jiang, *J. Controlled Release*, 2018, **274**, 56–68.

